New code for equilibriums and quasiequilibrium initial data of compact objects. III. Axisymmetric and triaxial rotating stars

Kōji Uryū,[1] Antonios Tsokaros,[2] Filippo Galeazzi,[2] Hideya Hotta,[1] Misa Sugimura,[1] Keisuke Taniguchi,[1] and Shin'ichirou Yoshida[3]

[1]*Department of Physics, University of the Ryukyus, Senbaru, Nishihara, Okinawa 903-0213, Japan*
[2]*Institut für Theoretische Physik, Johann Wolfgang Goethe-Universität, Max-von-Laue-Strasse 1, 60438 Frankfurt am Main, Germany*
[3]*Department of Earth Science and Astronomy, Graduate School of Arts and Sciences, University of Tokyo, Komaba, Tokyo 153-8902, Japan*

(Received 2 October 2015; published 23 February 2016)

We introduce new code for stationary and axisymmetric equilibriums, as well as for triaxial quasiequilibrium initial data, of single rotating relativistic stars. The new code is developed as a part of our versatile initial data code for compact objects, Compact Object CALculator (COCAL). In computing strong gravitational fields, the waveless formulation is incorporated into the COCAL code on top of the previously developed Isenberg-Wilson-Mathews formulation (conformally flat thin-sandwich formulation). Also introduced is a new differential rotation law that contains two parameters to control an angular velocity profile and a transition from uniform to differential rotation. We present convergence tests and solution sequences for both uniformly and differentially rotating equilibriums of stationary axisymmetric compact stars, as well as for quasiequilibrium initial data of uniformly rotating triaxial (nonaxisymmetric) compact stars. We also show comparisons of uniformly rotating axisymmetric solutions computed with three different codes: COCAL, LORENE, and the RNS code.

DOI: 10.1103/PhysRevD.93.044056

I. INTRODUCTION

The development of numerical methods for computing stationary axisymmetric equilibriums of relativistic rotating compact stars began over four decades ago, and some of them have been successfully applied for constructing rapidly rotating neutron stars and strange stars as models of pulsars [1–3]. (For reviews and complete references on rapidly rotating compact stars and their stability, see e.g. Ref. [4].) In this article, we introduce new code for computing such a single compact star in equilibrium or quasiequilibrium whose shape is highly deformed due to rapid rotation. The code is developed as part of the Compact Object CALculator (COCAL) code [5–8].

In most studies of numerical modeling of single rapidly rotating compact stars, it is commonly assumed that the perfect-fluid spacetime is stationary and axisymmetric, and the associated fluid flow is circular [4]. This ansatz is expected to be satisfied accurately for a rotating neutron star as a realistic model of a millisecond pulsar. In somewhat extreme situations such as newly born neutron stars or magnetars, however, one could imagine that axisymmetry or circularity may be violated even after those systems settle down to nearly stationary states [7,9,10]. Recent dynamical simulations in numerical relativity have confirmed that such compact objects may be produced as an outcome of stellar core collapses or binary neutron star mergers [11–14]. This motivates us to improve on the existing rotating neutron star codes specialized in computing solutions in circular spacetimes by our new COCAL code in which more general formulations are available for accurately modeling a variety of compact objects in equilibrium or in quasiequilibrium.

The COCAL project was started in Ref. [5] for computing the initial data of rotating compact stars on a spatially conformally flat hypersurface using the Isenberg-Wilson-Mathews (IWM) formulation [15,16]. In Ref. [5], data for axisymmetric as well as triaxial configurations of uniformly rotating stars—corresponding to classical Maclaurin and Jacobi ellipsoids in relativistic compressible self-gravitating fluid—were calculated successfully. In Ref. [6], multipatch coordinate grids were introduced for computing binary systems and applied for binary black hole initial data. In the development of the COCAL code, we restrict ourselves to using formulations and numerical methods as simple as possible, so that we are able to constantly update the code to include increasingly complex effects such as strong magnetic fields [7], realistic equations of state (EOSs) for high-density matter, or neutrino transfer and cooling in future works. One of the ideas for such simplification is to use the $3+1$ formalism similar to those used in the simulations for computing equilibriums or quasiequilibriums. This also allows us to conveniently provide various kinds of initial data for numerical relativity simulations. Those data are calculated in order to satisfy the initial value constraints on a three-dimensional hypersurface Σ_t; hence, they can be used as initial data as they are, or after certain density

or velocity perturbations are added and constraints are recalculated.[1]

In this paper, we introduce two new features of the COCAL code added to the above mentioned rotating compact star code; one is the waveless formulation for computing metric potentials, and the other is a novel differential rotation law. In contrast to IWM formalism, the waveless formulation derived in Ref. [18] (see also Ref. [19]) can describe stationary and axisymmetric spacetime exactly, whether or not the spacetime is circular. Differences between the solutions of uniformly rotating axisymmetric compact stars calculated from the IWM formalism and the exact stationary axisymmetric circular spacetime have been studied in Ref. [20]. They concluded that the differences between the two cases are not so evident as long as the compactness is in the range of neutron stars, $M/R \lesssim 0.2$. We present a result of the comparison for triaxially deformed stars with compactness up to $M/R \leq 0.3$. As an obvious caveat, such triaxially deformed compact stars are no longer in equilibrium due to the backreaction of gravitational waves, but they are quasiequilibrium initial data; these solutions satisfy the constraints and one or all components of the rest of Einstein's equations on a spatial hypersurface (depending on whether IWM or waveless formulation is used, respectively).

For the computations of differentially rotating compact stars, we introduce a novel rotation law which contains two parameters. One of the parameters, q, controls the slope of the angular velocity profile of differential rotation. In the Newtonian limit, this rotation law has an angular velocity dependence $\Omega \propto \varpi^{-2/q}$ on the equatorial radius ϖ. The other parameter, A, controls the transition radius between uniform rotation near the center of a star and the above differential rotation. Several authors have calculated differentially rotating compact stars using the rotation law $j(\Omega) = A(\Omega_c - \Omega)$, which corresponds to our $q = 1$ case [1,2]. To our knowledge, the only exception is the paper by Galeazzi, Yoshida, and Eriguchi [21], in which a rotation law analogous to ours is used. Our new rotation law has the same property as that of Ref. [21], but it has a simpler form so that it can always be analytically integrated in the equation of hydrostatic equilibrium. Recently, Mach and Malec have proposed more general differential rotation laws for relativistic rotating fluid bodies that involve four parameters [22], which are suited for reproducing the relativistic Keplerian rotation law. So far, they have not applied them for computing the equilibriums of rotating compact stars.

This paper is organized as follows: In Sec. II, the formulation of the problem, including a summary of the waveless formulation and the new differential rotation law, is introduced. In Sec. III, numerical methods and setups used in present computational code on COCAL are summarized. In Sec. IV, convergence tests and examples of solutions are presented for stationary axisymmetric differentially rotating compact stars and triaxially deformed rotating compact stars. Then properties of sequences of those solutions are investigated. We also present comparisons of two uniformly rotating axisymmetric solutions computed with three different codes, COCAL, LORENE, and the RNS code, one for a mildly compact and the other for a highly compact model. In Sec. V, we summarize the stability properties of rotating compact stars and discuss applications and future prospects of our new COCAL code. In this paper, spacetime indices are greek, spatial indices are latin, and the metric signature is $-+++$. For writing the basic equations, geometric units with $G = c = 1$ are used, while for tabulating the numerical solutions, $G = c = M_\odot = 1$ units are used for convenience.

II. FORMULATIONS

In this section, we introduce the $3+1$ decomposition of Einstein's equations, and the symmetry, the gauge conditions, and the waveless conditions to be imposed on the set of equations. Then, we summarize the waveless formulation [18,19], and the system of hydrostationary equations including the case with differential rotation.

A. Summary of $3+1$ decomposition of Einstein's equations

We assume that a spacetime $\mathcal{M}$ is asymptotically flat and is foliated by a family of spacelike hypersurfaces $(\Sigma_t)_{t\in\mathbb{R}}$, parametrized by a time coordinate $t \in \mathbb{R}$ as $\mathcal{M} = \mathbb{R} \times \Sigma$. The future-pointing unit normal one-form to Σ_t, $n_\alpha = -\alpha \nabla_\alpha t$, is related to the generator of time translations t^α as

$$t^\alpha = \alpha n^\alpha + \beta^\alpha, \tag{1}$$

where $t^\alpha \nabla_\alpha t = 1$. Above α and β^α are, respectively, the lapse and shift, where β^α is spatial, $\beta^\alpha \nabla_\alpha t = 0$. The projection tensor to Σ_t $\gamma^\alpha{}_\beta$ is introduced as $\gamma^\alpha{}_\beta := g^\alpha{}_\beta + n^\alpha n_\beta$. The induced spatial metric γ_{ab} on Σ_t is the projection tensor restricted to it. Introducing a conformal factor ψ, and a conformally rescaled spatial metric $\tilde{\gamma}_{ab}$, the line element on a chart $\{t, x^i\}$ of Σ_t is written

$$ds^2 = -\alpha^2 dt^2 + \psi^4 \tilde{\gamma}_{ij}(dx^i + \beta^i dt)(dx^j + \beta^j dt). \tag{2}$$

The conformal rescaling is determined from a condition $\tilde{\gamma} = f$, where $\tilde{\gamma}$ and f are determinants of the rescaled spatial metric $\tilde{\gamma}_{ab}$ and the flat metric f_{ab}, respectively. In the later sections, h_{ab} and h^{ab} denote the differences between the conformal metric and the flat one, with

[1]Such modification is often made for initial data sets for binary neutron stars or binary black holes to prepare the data of elliptic or parabolic orbits (see e.g. Ref. [17]).

$$\tilde{\gamma}_{ab} = f_{ab} + h_{ab}, \qquad \tilde{\gamma}^{ab} = f^{ab} + h^{ab}. \tag{3}$$

The extrinsic curvature of each slice Σ_t is defined by

$$\begin{aligned} K_{ab} &\coloneqq -\frac{1}{2}\gamma^{\alpha}{}_{a}\gamma^{\beta}{}_{b}\pounds_n\gamma_{\alpha\beta} \\ &= -\frac{1}{2\alpha}\partial_t\gamma_{ab} + \frac{1}{2\alpha}\pounds_\beta\gamma_{ab}, \end{aligned} \tag{4}$$

where $\partial_t\gamma_{ab}$ is the pullback of $\pounds_t\gamma_{\alpha\beta}$ to Σ_t, $\pounds_t$ is the Lie derivative along the vector t^α defined on $\mathcal{M}$, and $\pounds_\beta$ is the Lie derivative along the spatial vector β^a on Σ_t. Hereafter, we denote the trace of K_{ab} by K, and the trace-free part of K_{ab} by $A_{ab} \coloneqq K_{ab} - \frac{1}{3}\gamma_{ab}K$.

In this paper, we consider perfect-fluid spacetimes: the stress-energy tensor is written

$$T^{\alpha\beta} = (\epsilon + p)u^\alpha u^\beta + pg^{\alpha\beta}, \tag{5}$$

where ϵ is the energy density, p the pressure, and u^α the 4-velocity. We decompose Einstein's equation $\mathcal{E}_{\alpha\beta} \coloneqq G_{\alpha\beta} - 8\pi T_{\alpha\beta} = 0$ with respect to the foliation using hypersurface normal n^α, and the projection tensor γ^{ab} to Σ_t as follows:

$$\mathcal{E}_{\alpha\beta}n^\alpha n^\beta = 0, \tag{6}$$

$$\mathcal{E}_{\alpha\beta}\gamma^{\alpha}{}_{a}n^\beta = 0, \tag{7}$$

$$\mathcal{E}_{\alpha\beta}\left(\gamma^{\alpha\beta} + \frac{1}{2}n^\alpha n^\beta\right) = 0, \tag{8}$$

$$\mathcal{E}_{\alpha\beta}\left(\gamma^{\alpha}{}_{a}\gamma^{\beta}{}_{b} - \frac{1}{3}\gamma_{ab}\gamma^{\alpha\beta}\right) = 0, \tag{9}$$

which correspond, respectively, to the Hamiltonian constraint, the momentum constraint, the spatial trace part (combined with the Hamiltonian constraint), and the spatial trace-free part. As briefly reported in Ref. [7], the code can be extended to include the magnetic field.

B. Stationarity, waveless, and coordinate conditions

In the above set of field equations and the definition of the extrinsic curvature, the time-derivative terms $\partial_t\gamma_{ab}$, $\partial_t K_{ab}$, and $\partial_t K$ are included in Eqs. (4), (9), and (8), respectively.

1. Case A: Stationary and axisymmetric systems

For computing stationary and axisymmetric systems, we simply impose time symmetry by setting

$$\partial_t\gamma_{ab} = \partial_t K_{ab} = \partial_t K = 0 \tag{10}$$

under the maximal slicing and the generalized Dirac gauge for coordinate conditions,

$$K = 0, \tag{11}$$

$$\mathring{D}_b\tilde{\gamma}^{ab} = \mathring{D}_b h^{ab} = 0, \tag{12}$$

where $\mathring{D}_b$ is a covariant derivative associated with the flat spatial metric f_{ab}, $\mathring{D}_c f_{ab} = 0$. Note that we do not explicitly impose the axisymmetry on our formulation.

2. Case B: Nonaxisymmetric systems in quasiequilibrium

For computing quasiequilibrium initial data of triaxially deformed rotating stars, we impose a waveless condition on the rescaled metric $\tilde{\gamma}_{ab}$ and a stationarity in the rotating frame (helical symmetry) on the extrinsic curvature K_{ab},

$$\partial_t\tilde{\gamma}_{ab} = 0 \quad \text{and} \quad \partial_t K_{ab} = -\pounds_{\Omega\phi}K_{ab}, \tag{13}$$

under the same coordinate conditions. As shown in Ref. [18], a stronger waveless condition $\partial_t\tilde{\gamma}^{ab} = O(r^{-3})$ is sufficient for the metric potentials to fall off as Coulomb fields under the same coordinate conditions. For nonaxisymmetric stars, we do not consider differential rotations in this work. Hence, the star is stationary in a frame rotating with the constant angular velocity Ω of stellar rotation. This is a condition imposed on K_{ab} in Eq. (13) analogous to a symmetry with respect to a helical vector $k^\alpha = t^\alpha + \Omega\phi^\alpha$.

For either case A or case B above, the asymptotic behavior of the metric potentials becomes a Coulomb-type falloff,

$$\psi - 1 = O(r^{-1}), \qquad \alpha - 1 = O(r^{-1}), \tag{14}$$

$$\beta^a = O(r^{-2}), \qquad h_{ab} = O(r^{-1}). \tag{15}$$

Our choice of β^a is the shift in an (asymptotically) inertial frame.

Also, the trace-free part A_{ab} of the extrinsic curvature (4) becomes

$$A_{ab} = \frac{\psi^4}{2\alpha}\left(\pounds_\beta\tilde{\gamma}_{ab} - \frac{1}{3}\tilde{\gamma}_{ab}\tilde{\gamma}^{cd}\pounds_\beta\tilde{\gamma}_{cd}\right). \tag{16}$$

The trace part of (4) determines the evolution of the conformal factor under the slicing condition $K = 0$, which is not necessary for computing the stationary system or the initial data.

C. Equations for the metric potentials

As shown in Ref. [18], the above set of field equations (6)–(9) are reduced to elliptic (Poisson) equations for $\{\psi, \tilde{\beta}_a, \alpha\psi, h_{ab}\}$, respectively, as follows:

$$\mathring{\Delta}\psi = \mathcal{S}_{\rm H}, \tag{17}$$

$$\mathring{\Delta}\tilde{\beta}_a = \mathcal{S}_a, \tag{18}$$

$$\mathring{\Delta}(\alpha\psi) = \mathcal{S}_{\rm tr}, \tag{19}$$

$$\mathring{\Delta}h_{ab} = \mathcal{S}_{ab}, \tag{20}$$

where $\mathring{\Delta}$ is defined by $\mathring{\Delta} = f^{ab}\mathring{D}_a\mathring{D}_b$, and the conformally rescaled shift $\tilde{\beta}_a$ by $\tilde{\beta}_a = \tilde{\gamma}_{ab}\tilde{\beta}^b$, $\tilde{\beta}^a = \beta^a$. The sources $\mathcal{S}_{\rm H}$, $\mathcal{S}_a$, $\mathcal{S}_{\rm tr}$, and $\mathcal{S}_{ab}$ are written

$$\begin{aligned}\mathcal{S}_{\rm H} :=& -h^{ab}\mathring{D}_a\mathring{D}_b\psi + \tilde{\gamma}^{ab}C^c_{ab}\mathring{D}_c\psi + \frac{\psi}{8}{}^3\tilde{R} \\ & - \frac{\psi^5}{8}\left(\tilde{A}_{ab}\tilde{A}^{ab} - \frac{2}{3}K^2\right) - 2\pi\psi^5\rho_{\rm H},\end{aligned} \tag{21}$$

$$\begin{aligned}\mathcal{S}_a :=& -h^{bc}\mathring{D}_b\mathring{D}_c\tilde{\beta}_a + \tilde{\gamma}^{bc}\mathring{D}_b(C^d_{ca}\tilde{\beta}_d) + \tilde{\gamma}^{bc}C^d_{bc}\tilde{D}_d\tilde{\beta}_a \\ & + \tilde{\gamma}^{bc}C^d_{ba}\tilde{D}_c\tilde{\beta}_d - \frac{1}{3}\mathring{D}_a(h^{bc}\mathring{D}_b\tilde{\beta}_c - \tilde{\gamma}^{bc}C^d_{bc}\tilde{\beta}_d) \\ & - \frac{1}{3}\mathring{D}_a\mathring{D}^b\tilde{\beta}_b - {}^3\tilde{R}_{ab}\tilde{\beta}^b - 2\alpha\tilde{A}_a{}^b\frac{\alpha}{\psi^6}\tilde{D}_b\left(\frac{\psi^6}{\alpha}\right) \\ & + \frac{4}{3}\alpha\tilde{D}_aK + 16\pi\alpha j_a,\end{aligned} \tag{22}$$

$$\begin{aligned}\mathcal{S}_{\rm tr} :=& -h^{ab}\mathring{D}_a\mathring{D}_b(\alpha\psi) + \tilde{\gamma}^{ab}C^c_{ab}\mathring{D}_c(\alpha\psi) + \frac{\alpha\psi}{8}{}^3\tilde{R} \\ & + \psi^5\pounds_\omega K + \alpha\psi^5\left(\frac{7}{8}\tilde{A}_{ab}\tilde{A}^{ab} + \frac{5}{12}K^2\right) \\ & + 2\pi\alpha\psi^5(\rho_{\rm H} + 2S),\end{aligned} \tag{23}$$

$$\mathcal{S}_{ab} := 2\bar{\mathcal{S}}^{\rm TF}_{ab} - \frac{1}{3}\tilde{\gamma}_{ab}\mathring{D}^e h^{cd}\mathring{D}_e h_{cd}, \tag{24}$$

where $\bar{\mathcal{S}}^{\rm TF}_{ab}$ in Eq. (24) is a trace-free part of $\bar{\mathcal{S}}_{ab}$, which is

$$\begin{aligned}\bar{\mathcal{S}}_{ab} :=& \tilde{R}^{\rm D}_{ab} + \tilde{R}^{\rm NL}_{ab} + {}^3\bar{R}^\psi_{ab} - \frac{1}{\alpha}\bar{D}_a\bar{D}_b\alpha \\ & + \frac{1}{3}\psi^4K\tilde{A}_{ab} - 2\psi^4\tilde{A}_{ac}\tilde{A}_b{}^c \\ & + \frac{1}{\alpha}\pounds_\omega(\psi^4\tilde{A}_{ab}) - 8\pi\bar{S}_{ab}.\end{aligned} \tag{25}$$

Here, ω^a is a rotating shift defined by $\omega^a = \beta^a + \Omega\phi^a$. The conformal weighted quantity $\tilde{A}_{ab}$ is defined by $\tilde{A}_a{}^b := A_a{}^b$, and its indices are raised (lowered) by the rescaled metric $\tilde{\gamma}^{ab}$ ($\tilde{\gamma}_{ab}$). $\tilde{D}_a$ is a covariant derivative of the conformally rescaled spatial metric $\tilde{\gamma}_{ab}$, and C^c_{ab} is a connection associated with $\tilde{D}_a$. ${}^3\tilde{R}_{ab}$ and ${}^3\tilde{R}$ are, respectively, the conformal Ricci tensor and scalar of the conformal spatial hypersurface whose intrinsic metric is the rescaled $\tilde{\gamma}_{ab}$. Definitions of $\tilde{R}^{\rm D}_{ab}$, $\tilde{R}^{\rm NL}_{ab}$, and ${}^3\bar{R}^\psi_{ab} - \frac{1}{\alpha}\bar{D}_a\bar{D}_b\alpha$ follow:

$$\tilde{R}^{\rm D}_{ab} = -\frac{1}{2}(f_{ac}\mathring{D}_bF^c + f_{bc}\mathring{D}_aF^c), \tag{26}$$

$$\begin{aligned}\tilde{R}^{\rm NL}_{ab} =& -\frac{1}{2}(\mathring{D}_bh^{cd}\mathring{D}_ch_{ad} + \mathring{D}_ah^{cd}\mathring{D}_ch_{bd} + h^{cd}\mathring{D}_c\mathring{D}_dh_{ab}) \\ & - \mathring{D}_aC^c_{cb} + C^c_{ab}C^d_{dc} - C^d_{ac}C^c_{bd} \\ & - \frac{1}{2}[\mathring{D}_b(h_{ac}F^c) + \mathring{D}_a(h_{bc}F^c)] + F^cC_{c,ab},\end{aligned} \tag{27}$$

$$\begin{aligned}{}^3\bar{R}^\psi_{ab} - \frac{1}{\alpha}\bar{D}_a\bar{D}_b\alpha =& -\frac{1}{\alpha\psi^2}\mathring{D}_a\mathring{D}_b(\alpha\psi^2) + \frac{1}{\alpha\psi^2}C^c_{ab}\mathring{D}_c(\alpha\psi^2) \\ & + \frac{4}{\alpha\psi^2}[\mathring{D}_a(\alpha\psi)\mathring{D}_b\psi + \mathring{D}_b(\alpha\psi)\mathring{D}_a\psi],\end{aligned} \tag{28}$$

where $F^a := \mathring{D}_b\tilde{\gamma}^{ab} = \mathring{D}_bh^{ab}$ and $C_{c,ab} := \tilde{\gamma}_{cd}C^d_{ab}$. The condition $\tilde{\gamma} = f$ and the generalized Dirac gauge condition (12) imply, respectively, $C^b_{ba} = 0$ and $F^a = 0$.

We comment on two subtle differences in the formulation between our previous and present codes. In the previous code (e.g. Refs. [5,19]), a term $-\frac{1}{3}\mathring{D}_a\mathring{D}^b\tilde{\beta}_b$ appearing in the third line of Eq. (22) was calculated separately using a decomposition of β_a (see Appendix A of Ref. [19]). We no longer use such a decomposition but include the term in the source (22) and simply solve Eq. (18). We had also used an analogous decomposition in solving a gauge vector ξ_a in Ref. [19], but we no longer use it either. As explained in Ref. [19], the Dirac gauge condition (12) is imposed on h_{ab} by a simultaneous gauge transformation at each level of a self-consistent iteration to solve field equations (17)–(20). Namely, gauge vector potentials ξ^a introduced in the transformation

$$\delta\gamma^{ab} \to \delta\gamma^{ab} - \mathring{D}^a\xi^b - \mathring{D}^b\xi^a \tag{29}$$

are used to adjust h^{ab} as

$$h^{ab\prime} = h^{ab} - \mathring{D}^a\xi^b - \mathring{D}^b\xi^a + \frac{2}{3}f^{ab}\mathring{D}_c\xi^c, \tag{30}$$

in order to have $h^{ab\prime}$ satisfy the condition $\mathring{D}_bh^{ab\prime} = 0$. Then, the gauge vector potentials ξ^a are solved from elliptic equations,

$$\mathring{\Delta}\xi^a = \mathcal{S}^a_{\rm D}, \tag{31}$$

$$\mathcal{S}^a_{\rm D} = \mathring{D}_bh^{ab} - \frac{1}{3}\mathring{D}^a\mathring{D}_b\xi^b, \tag{32}$$

and h_{ab} is replaced by Eq. (30).

Terms $\rho_{\rm H}$, j_a, S, and S_{ab} in the source (21)–(24) correspond to the projection of the stress energy tensor (5) with respect to the slices Σ_t and to its normal. The 4-velocity of the flow

$$u^\alpha = u^t(t^\alpha + v^\alpha), \tag{33}$$

where v^α is the spatial vector $v^\alpha n_\alpha = 0$, is decomposed into

$$u^\alpha n_\alpha = -\alpha u^t, \tag{34}$$

$$u_\alpha \gamma^\alpha{}_a = u^t(\beta_a + v_a). \tag{35}$$

Using these relations, the matter source terms of the field equations are written

$$\rho_{\rm H} := T_{\alpha\beta} n^\alpha n^\beta = h\rho(\alpha u^t)^2 - p, \tag{36}$$

$$j_a := -T_{\alpha\beta}\gamma^\alpha{}_a n^\beta = h\rho\alpha(u^t)^2(\beta_a + v_a), \tag{37}$$

$$S := T_{\alpha\beta}\gamma^{\alpha\beta} = h\rho[(\alpha u^t)^2 - 1] + 3p, \tag{38}$$

$$S_{ab} := T_{\alpha\beta}\gamma^\alpha{}_a\gamma^\beta{}_b = h\rho(u^t)^2(\beta_a + v_a)(\beta_b + v_b) + p\gamma_{ab}, \tag{39}$$

where ρ is the rest mass density and h the relativistic enthalpy defined by

$$h := \frac{\epsilon + p}{\rho}. \tag{40}$$

In this paper, we concentrate on the case with the circular flow $v^\alpha = \Omega\phi^\alpha$, although we have already included the components of meridional flow in the source of the field equation in the COCAL code as above.

The above formulation is reduced to the IWM formulation by setting the spatial metric to be conformally flat, $\gamma_{ab} = \psi^4 f_{ab}$—that is, by replacing

$$\tilde{\gamma}_{ab} \to f_{ab}, \qquad \tilde{D}_a \to \mathring{D}_a, \tag{41}$$

$$h_{ab},\ C^c_{ab},\ {}^3\tilde{R}_{ab},\ {}^3\tilde{R},\ \tilde{R}^{\rm D}_{ab},\ \tilde{R}^{\rm NL}_{ab} \to 0, \tag{42}$$

then discarding the field equations (20) for h_{ab}. Further details for deriving the equations in this subsection can be found in Refs. [18,19].

D. Equations for hydrostationary (quasi)equilibriums

For the properties of high-density matter, we consider the case in which the local thermodynamic equilibrium is always satisfied, and is described by two independent thermodynamic quantities which we choose to be the rest mass density ρ and entropy per rest mass density s, such as $\epsilon = \epsilon(\rho, s)$ and $p = p(\rho, s)$. The first law of thermodynamics is written $d\epsilon = \rho T ds + h d\rho$, where the relativistic enthalpy h is defined as in Eq. (40).

The Bianchi identity implies $\nabla_\beta T_\alpha{}^\beta = 0$; that is, for the case of a perfect fluid (5),

$$\nabla_\beta T_\alpha{}^\beta = \rho u^\beta \omega_{\beta\alpha} + h u_\alpha \nabla_\beta(\rho u^\beta) - \rho T \nabla_\alpha s = 0, \tag{43}$$

where $\omega_{\beta\alpha} := \nabla_\beta(hu_\alpha) - \nabla_\alpha(hu_\beta)$ is the relativistic vorticity two-form. In this derivation, the normalization condition of the 4-velocity $u^\alpha u_\alpha = -1$ and the local first law in the form $dh = Tds + dp/\rho$ are used.

The assumption for the local baryon mass conservation,

$$\nabla_\alpha(\rho u^\alpha) = 0, \tag{44}$$

implies the isentropic flow and the relativistic Euler equation

$$u^\alpha \nabla_\alpha s = 0, \tag{45}$$

$$u^\beta \omega_{\beta\alpha} - T\nabla_\alpha s = 0, \tag{46}$$

from projections of Eq. (43) along, and transverse to, the fluid flow u^α, respectively.

The above set of equations (44)–(46), together with the equations of state (EOSs) of high-density matter,

$$p = p(\rho, s), \tag{47}$$

[or $h = h(\rho, s)$], and a normalization condition of the 4-velocity,

$$u_\alpha u^\alpha = -1, \tag{48}$$

are the closed system of equations for relativistic perfect fluid. For computing equilibriums or quasiequilibriums of self-gravitating fluid, it is crucial to find a set of integrability conditions and to derive a system of first integrals of the above system.

1. Stationary and axisymmetric systems with circular flow

Stationarity and axisymmetry are imposed on the canonical momentum of fluid element hu_α and thermodynamic variables as their Lie derivatives along the Killing fields t^α and ϕ^α vanish:

$$\pounds_t(hu_\alpha) = 0, \qquad \pounds_t\rho = 0, \qquad \pounds_t s = 0, \tag{49}$$

$$\pounds_\phi(hu_\alpha) = 0, \qquad \pounds_\phi\rho = 0, \qquad \pounds_\phi s = 0. \tag{50}$$

We assume the flow is circular,

$$u^\alpha = u^t k^\alpha = u^t(t^\alpha + \Omega\phi^\alpha), \tag{51}$$

where the angular velocity Ω may not necessarily be constant. Conditions (49) and (50) imply $\pounds_t\Omega = 0$ and $\pounds_\phi\Omega = 0$. Also, using the same conditions, Eqs. (44) and (45) are trivially satisfied. The Euler equation (46) becomes

$$\nabla_\alpha \ln\frac{h}{u^t} + u^t u_\phi \nabla_\alpha\Omega - \frac{T}{h}\nabla_\alpha s = 0, \tag{52}$$

since Cartan identity implies

$$k^\beta \omega_{\beta\alpha} = \pounds_k(hu_\alpha) - \nabla_\alpha(hu_\beta k^\beta) = hu_\beta \phi^\beta \nabla_\alpha \Omega - \nabla_\alpha(hu_\beta k^\beta). \tag{53}$$

Equation (52) suggests that the first integral can be derived if the combination $u^t u_\phi$ is a function of Ω, and T/h a function of s. For the latter, we assume barotropic fluid, $s = s(\rho)$, and hence, we have $p = p(\rho, s(\rho))$, $\epsilon = \epsilon(\rho, s(\rho))$ as well as other thermodynamic quantities. Writing

$$j(\Omega) := u^t u_\phi, \tag{54}$$

the first integral is written

$$\ln \frac{h}{u^t} + \int j(\Omega) d\Omega - \int \frac{T}{h} ds = \text{const.} \tag{55}$$

In this paper, we further simplify that the flow is homentropic, and therefore solve

$$\frac{h}{u^t} \exp\left[\int j(\Omega) d\Omega\right] = \mathcal{E}, \tag{56}$$

where $\mathcal{E}$ is a constant.

A choice of the form of integrability function $j(\Omega)$ amounts to a choice of a differential rotation law. Several authors have calculated differentially rotating compact stars using the rotation law $j(\Omega) = A(\Omega_c - \Omega)$, except for Ref. [21]. We propose a generalized differential rotation law, which can cover various rotation laws by two parameters, and is simple enough to implement in the code. The integrability function $j(\Omega)$ is given as

$$j(\Omega) := A^2 \Omega \left[\left(\frac{\Omega_c}{\Omega}\right)^q - 1\right], \tag{57}$$

where A and q are parameters, and Ω_c is a constant. The function $j(\Omega)$ (57) can be immediately integrated analytically as

$$\int j(\Omega) d\Omega = \begin{cases} A^2\Omega^2 \left[\frac{1}{2-q}\left(\frac{\Omega_c}{\Omega}\right)^q - \frac{1}{2}\right], & \text{for } q \neq 2, \\ A^2\Omega^2 \left[\left(\frac{\Omega_c}{\Omega}\right)^2 \ln \Omega - \frac{1}{2}\right], & \text{for } q = 2. \end{cases} \tag{58}$$

In actual computation, we subtract from Eq. (58) the integral constants $A^2\Omega_c^2 q/(4-2q)$ and $A^2\Omega_c^2(\ln \Omega_c - 1/2)$ for $q \neq 2$ and $q = 2$, respectively, to have the integrals (58) vanish when $\Omega = \Omega_c$. The value of Ω is solved from a relation $j(\Omega) = u^t u_\phi$, where $u^t u_\phi$ is concretely

$$u^t u_\phi = (u^t)^2 \gamma_{\alpha\beta} \omega^\alpha \phi^\beta = (u^t)^2 \psi^4 \tilde{\gamma}_{ab} \omega^a \phi^b, \tag{59}$$

where the spatial vector ω^α is defined by $\omega^\alpha = \beta^\alpha + \Omega\phi^\alpha$, and ω^a is its projection to Σ_t. Properties of this new differential rotation law (57) are detailed later in Sec. IV A 1.[2]

Finally, u^t is determined from the normalization condition (48), which is written

$$u^t = \frac{1}{\sqrt{-g_{\alpha\beta} k^\alpha k^\beta}} = \frac{1}{\sqrt{\alpha^2 - \psi^4 \tilde{\gamma}_{ab} \omega^a \omega^b}}. \tag{60}$$

In summary, the number of independent fluid variables $\{\rho, s, u^\alpha\}$ is reduced to $\{h, u^t\}$ and two constants $\{\Omega_c, \mathcal{E}\}$, and accordingly the system of equations (44)–(48) is reduced to the first integral and the integrability condition (the rotation law) (55) or (56) to (60), and an associated EOS whose example is discussed below in Sec. II D 3.

2. Nonaxisymmetric systems in quasiequilibrium

For quasiequilibrium initial data of rotating nonaxisymmetric compact objects, we only consider the case with uniform rotation. Hence, the fluid 4-velocity u^α is proportional to a helical vector $k^\alpha = t^\alpha + \Omega\phi^\alpha$, $u^\alpha = u^t k^\alpha$, where Ω is a constant angular velocity of the rotation. Then, we assume that the canonical momentum of a fluid particle hu_α and thermodynamic variables respect the helical symmetry,

$$\pounds_k(hu_\alpha) = 0, \qquad \pounds_k \rho = 0, \qquad \pounds_k s = 0. \tag{61}$$

In this case, the Cartan identity for the helical Killing vector k^α becomes

$$k^\beta \omega_{\beta\alpha} = -\nabla_\alpha(hu_\alpha k^\alpha), \tag{62}$$

and hence, analogously to the differentially rotating axisymmetric case above, we have the first integral for barotropic fluid

$$\ln \frac{h}{u^t} - \int \frac{T}{h} ds = \text{const.} \tag{63}$$

in place of Eq. (55), and for the homentropic case

$$\frac{h}{u^t} = \mathcal{E} \tag{64}$$

in place of Eq. (56). One of Eqs. (63) or (64), and Eq. (60) are solved for $\{h, u^t\}$, and two constants $\{\Omega, \mathcal{E}\}$ are to be determined.

We remind the readers again that the terms "helical symmetry" and "helical Killing vector" do not mean

[2]The properties of our new rotation law are essentially the same as those of Ref. [21]. Note that the definition of a function $j(\Omega)$ in Ref. [21] differs from our definition of $j(\Omega)$.

spacetime symmetry, but a condition imposed only on the fluid variables.

3. Piecewise polytropic EOS

As a concrete form of barotropic EOS, we adopt a piecewise polytropic EOS with N segments [23],

$$p = K_i \rho^{\Gamma_i}, \tag{65}$$

in the ith interval $\rho \in [\rho_{i-1}, \rho_i]$, $i = 1, \ldots, N$. The adiabatic constant and the adiabatic index (K_i, Γ_i) are assigned parameters to each density interval $[\rho_{i-1}, \rho_i]$, and the values of the density at the interface ρ_i satisfy $\rho_i < \rho_{i+1}$. We have N parameters each of K_i and Γ_i, and $N-1$ parameters of ρ_i, hence in total $3N-1$ degrees of freedom for the N-segment piecewise polytropic EOS. A requirement that the pressure $p(\rho)$ be continuous at each interface ρ_i gives $N-1$ conditions to the above parameters:

$$K_i \rho_i^{\Gamma_i} = K_{i+1} \rho_i^{\Gamma_{i+1}} \quad (i = 1, \ldots, N-1), \tag{66}$$

which determine $N-1$ values of K_i. The remaining $2N$ parameters—N values of Γ_i, $N-1$ values of ρ_i, and one of K_i—are prescribed. Instead of the one of K_i, we may also prescribe the value of p at a certain value of ρ.

In COCAL code, we store the value of the thermodynamic quantity $q := p/\rho$ and reconstruct other thermodynamic variables in the ith interval as follows[3]:

$$h = h_i + \frac{\Gamma_i}{\Gamma_i - 1}(q - q_i), \tag{67}$$

$$p = K_i^{\frac{-1}{\Gamma_i - 1}} q^{\frac{\Gamma_i}{\Gamma_i - 1}}, \quad \text{and} \quad \rho = K_i^{\frac{-1}{\Gamma_i - 1}} q^{\frac{1}{\Gamma_i - 1}}, \tag{68}$$

where q_i and h_i are the values at the interface of the ith and $(i+1)$th intervals, and an interval $q \in [q_{i-1}, q_i]$ corresponds to $[\rho_{i-1}, \rho_i]$ with $i = 1, \ldots, N$. We assume $\Gamma_1 > 1$ so that we may set $p_0 = \rho_0 = q_0 = 0$ and $h_0 = 1$ consistently at the boundary of the first interval.

Parametrization of various high-density nuclear EOSs using the above piecewise polytropic EOS with a minimal number of intervals has been studied by Read *et al.* in Ref. [24]. They systematically fit the EOS of neutron-star matter with three intervals plus one fixed interval for the crust.

III. SUMMARY OF NUMERICAL METHOD

In the COCAL project, we aim at developing a versatile code for computing compact objects as simply as possible, so that extensions for solving increasingly complex problems can be done with minimal extra effort. The code for solving the waveless formulation, in fact, has been developed on top of that for the IWM formulation [5] by adding extra terms related to conformally rescaled spatial metric $\tilde{\gamma}_{ab}$. As in our previous code [5,6,19], we solve Cartesian components of the field equations on spherical coordinate grids in our numerical computations. Therefore, a basis of numerical setups in the present code is mostly common with that of Ref. [5]. We briefly review it in this section.

A. Coordinate grids, finite differencing, and other numerical schemes of the COCAL code

As in Ref. [5], for computing a single rotating star, the spherical coordinates cover the region $(r, \theta, \phi) \in [r_a, r_b] \times [0, \pi] \times [0, 2\pi]$. For a rotating star computation, r_a is set to zero and r_b typically to $r_b \sim O(10^6 M)$, where M is the total mass of the system. Definitions of the parameters for the grid setups are listed in Table I.

Using a Green's function, an integral form of each of the elliptic equations (17)–(20) for the metric potentials is written. We apply the same finite difference scheme used in Ref. [6] to discretize these integral equations on the spherical coordinates: (1) For the quadrature formula of the Poisson solver, a second-order midpoint rule is used for r and ϕ integrations, and a fourth-order midpoint rule is used for θ integration. (2) A second-order finite difference formula is used for the r, θ, and ϕ derivatives evaluated at the midpoints $(r_{i+\frac{1}{2}}, \theta_{j+\frac{1}{2}}, \phi_{k+\frac{1}{2}}) = ((r_i + r_{i+1})/2, (\theta_i + \theta_{i+1})/2, (\phi_i + \phi_{i+1})/2)$, except that (3) a third-order finite difference formula is used for the first derivative in r evaluated at the midpoints. (4) A fourth-order finite difference formula is used for the derivatives evaluated at the grid points, (r_i, θ_j, ϕ_k). Note that we use the midpoint rule for the numerical quadrature formula, and hence compute the source terms at the midpoints of the grids.

Coordinate grids (r_i, θ_j, ϕ_k) with $i = 0, \ldots, N_r$, $j = 0, \ldots, N_\theta$, and $k = 0, \ldots, N_\phi$ are freely specifiable except for the first and the last grid points of the computational domain. The grid setup is the same as that in Ref. [5]: the radial grid intervals $\Delta r_i := r_i - r_{i-1}$ are constant between $r_i \in [r_a, r_c]$ $(i = 1, \ldots, N_r^{\mathrm{m}})$ and increase proportionally, $\Delta r_i = k \Delta r_{i-1}$, where k is a constant, between

TABLE I. Summary of grid parameters.

r_a: Radial coordinate where the radial grids start.
r_b: Radial coordinate where the radial grids end.
r_c: Radial coordinate between r_a and r_b where the radial grid spacing changes.
N_r: Number of intervals Δr_i in $r \in [r_a, r_b]$.
N_r^{f}: Number of intervals Δr_i in $r \in [r_a, 1]$.
N_r^{m}: Number of intervals Δr_i in $r \in [r_a, r_c]$.
N_θ: Number of intervals $\Delta\theta_j$ in $\theta \in [0, \pi]$.
N_ϕ: Number of intervals $\Delta\phi_k$ in $\phi \in [0, 2\pi]$.
L: Order of included multipoles.

[3]We use q for $q := p/\rho$ only in this subsection. Here, q may be considered as a relativistic Emden function.

TABLE II. Grid parameters used for computing rotating compact stars.

Type	r_a	r_b	r_c	$N_r^{\rm f}$	$N_r^{\rm m}$	N_r	N_θ	N_ϕ	L
H1	0.0	10^6	1.25	32	40	96	24	24	12
H2	0.0	10^6	1.25	64	80	192	48	48	12
H3	0.0	10^6	1.25	128	160	384	96	96	12
H4	0.0	10^6	1.25	256	320	768	192	192	12

$r_i \in [r_c, r_b]$ $(i = N_r^{\rm m}+1, \ldots, N_r)$. For angular coordinate grids (θ_j, ϕ_k), we choose equally spaced grids.

Values of the parameters for the coordinate grids of COCAL used in computing the results presented in this paper are listed in Table II.

B. Iteration scheme and a number of parameters to specify a solution

In the COCAL code, all components of field equations become elliptic PDEs (17)–(20), and they are recast into integral forms using Green's function [5,6]. These integral equations, a hydrostatic equation (56) or (64), and a normalization of 4-velocity (60), associated with a certain barotropic EOS such as (65), are simultaneously solved iteratively by a self-consistent field method [25]. As discussed in Ref. [26], to achieve a successful convergence of such iterations to compute stellar equilibriums, parameters to specify a solution should be chosen appropriately. In the hydrostatic equations, free constants $\{\mathcal{E}, \Omega\}$ (or $\{\mathcal{E}, \Omega_c\}$ for the case of differential rotation) are to be computed during iterations. We also introduce a parameter R_0 to normalize lengths, so that the stellar equatorial radius R_e (along the x axis) becomes unity.[4]

To determine $\{\mathcal{E}, \Omega, R_0\}$ (or $\{\mathcal{E}, \Omega_c, R_0\}$), we fix three conditions: the equatorial coordinate radius $R_e/R_0 = 1$, the axis ratio R_p/R_0, and the maximum value of $(p/\rho)_c$. Here, R_p is the polar radius measured in coordinate length.[5] These conditions are substituted into the hydrostatic equation (56) [or (64)] at the pole, the equatorial surface (on the x axis), and at the center or at the point of the maximum of p/ρ. A solution is specified by the values of the above three parameters, and the values of other parameters included in the EOS $\{\Gamma_i, K_i\}$ and the differential rotation law $\{q, A\}$.

IV. NUMERICAL RESULTS

In this section, we show the structures of two representative solutions, the results of convergence tests, and the results of systematic computations for solution sequences. Although a piecewise polytropic EOS is already available in COCAL, we use the polytropic EOS $p = K\rho^\Gamma$ (the EOS composed of only one segment) in the following computations. We choose the adiabatic index Γ to be either 2, 3, or 4, and for each case choose the adiabatic constant K so that the compactness of a TOV solution with the rest mass $M_0 = 1.5 M_\odot$ becomes $M/R = 0.2$. Throughout this paper, the definition of the compactness M/R of a rotating compact star is the ratio of the gravitational mass M to the circumferential (Schwarzschild) radius R of the corresponding spherical TOV solution having the same rest mass M_0 as the rotating star, as long as the mass of the rotating star does not exceed the maximum mass of the TOV solution. As a reference, the quantities of TOV solutions at the maximum mass for the above Γ are tabulated in Table III.

TABLE III. Quantities of a TOV solution in $G = c = M_\odot = 1$ units for the polytropic EOS $p = K\rho^\Gamma$ with $\Gamma = 2$, 3, and 4. $(p/\rho)_c$ and ρ_c are the maximum values of each quantity. M_0 is the rest mass, M is the gravitational mass, and M/R is the compactness (a ratio of the gravitational mass to the circumferential radius). The first three lines are the maximum mass models of the corresponding EOS parameters. The adiabatic constant K is chosen so that the value of M_0 becomes $M_0 = 1.5$ at the compactness $M/R = 0.2$. Values are approximated using second-order interpolation of three nearby solutions. To convert a unit of ρ_c to cgs, multiply the values by $M_\odot (G M_\odot/c^2)^{-3} \approx 6.176393 \times 10^{17}$ g cm^{-3}.

Γ	$(p/\rho)_c$	ρ_c	M_0	M	M/R
2	0.318244	0.00448412	1.51524	1.37931	0.214440
3	0.827497	0.00415972	2.24295	1.84989	0.316115
4	1.330409	0.00322082	2.88207	2.24967	0.355062
4	0.062524	0.00116231	0.58996	0.55484	0.1
4	0.178842	0.00164991	1.50000	1.31353	0.2
4	0.499659	0.00232378	2.51730	2.03208	0.3

A. Examples of highly deformed rotating compact stars

First, we present two examples of solutions for highly deformed rotating compact stars. One is a differentially rotating axisymmetric star in equilibrium, and the other a uniformly rotating triaxial star in quasiequilibrium. Both solutions are computed using the waveless formulation. Before presenting these solutions, we comment on properties of our differential rotation law (57).

1. Differential rotation for a compact star

In Fig. 1, we plot analytic solutions of the rotation law in the Newtonian limit $j(\Omega) = \varpi^2 \Omega$,

$$\Omega = \Omega_c \left(\frac{\varpi^2}{A^2} + 1 \right)^{-1/q}, \tag{69}$$

[4]In the actual numerical code, the equations in our formulation are normalized by R_0 accordingly, which we do not repeat here, as we have fully discussed it in our previous papers [5,27].

[5]In later sections, we also use R_x, R_y, and R_z as radii along the x, y, and z axes (length of semiprincipal axes), where $R_x = R_e = R_0$ and $R_z = R_p$. For axisymmetric stars, R_y is equal to R_0 also.

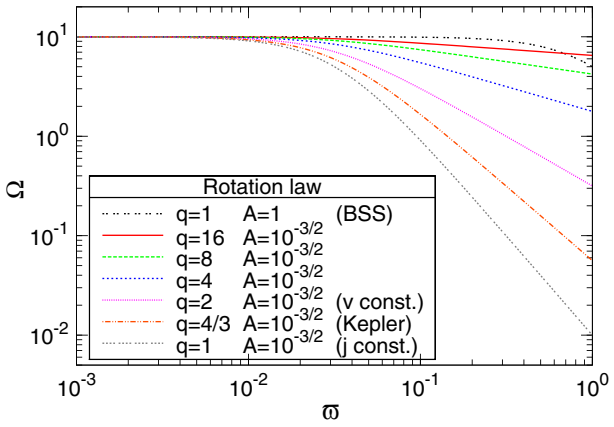

FIG. 1. Plot for the angular velocity Ω along the radial coordinate $\varpi(=r\sin\theta)$ of the cylindrical coordinates in the Newtonian limit. Curves are solutions of $j(\Omega)=\varpi^2\Omega$, where $j(\Omega)$ is defined by the rotation law (57). The parameter q controls the slope $\Omega\sim\varpi^{-2/q}$, and the parameter A/R_0 controls the transition radius from uniform to differential rotation. In this figure, we set $A^2=10^{-3}$ so that the transition occurs around $\varpi\sim A\sim 0.03$, except for one case with $A^2=1$. The cases $q=1$, 1.5, and 2, with a small A correspond, respectively, to j-constant, Kepler, and v-constant laws. The parameter set $A^2=1$ and $q=1$ is used by Baumgarte, Shapiro, and Shibata (BSS) [28] for computing hypermassive solutions. In these examples, we set $\Omega_c=10$.

along a radial coordinate $\varpi(=r\sin\theta)$ of cylindrical coordinates, for several parameters $\{q,A\}$. As seen in these figures, the above rotation law is chosen to avoid a singular behavior of Ω near the rotation axis of the star: the parameter A controls a point of transition from a constant $\Omega\sim\Omega_c$ to a differential rotation. This transition from rigid to differential rotation occurs around $\varpi\sim A/R_0$. The parameter q controls a slope of Ω as $\Omega\sim\varpi^{-2/q}$ in the Newtonian limit. In the Newtonian limit with a value A substantially smaller than the stellar radius R_0, the rotation law (57) with the parameter $q=1$ tends to the specific angular momentum constant (j-constant) law, with $q=2$ corresponding to the rotational velocity constant (v-constant) law, and with $q=4/3$ corresponding to Kepler's law. Note that in the case of strong gravity, rotation laws may not tend to v-constant or Kepler laws for $q=2$, or $4/3$.

Most of the differential rotation laws used in computations of compact stars in the literature (e.g. Ref. [1]) are the case with $q=1$ of our new rotation law (57), except for the recent work by Galeazzi, Yoshida, Eriguchi in Ref. [21]. Differentially rotating solutions of compact objects have attracted attention because of the discovery of differentially rotating hypermassive neutron stars as remnants of binary neutron star mergers [13]. Baumgarte, Shapiro, and Shibata [28] (hereafter, BSS), and later Morrison [29] have found that the differential rotation can sustain even twice as much as the maximum mass of the TOV star.[6] In these studies, the rotation parameter is fixed at $q=1$, and A is varied in a range $\sim 0.5-1$. Galeazzi *et al.* [21] extended these works to improve the modeling of merger remnants with more realistic rotation profiles.

The behavior of our new differential rotation law is similar to that of Galeazzi *et al.* [21]. In fact, the number of free parameters in both rotation laws is the same, and therefore our rotation law is as flexible as that of Ref. [21]. Because the form of our rotation law is simpler, it is straightforward to implement in the code, and it may be easier to modify it to introduce rotation laws with multiple slopes if necessary. Recent numerical simulations suggest that more complex differential rotation profiles may be realized in binary merger remnants [31]. Our code will be useful for modeling such objects in the future.

2. Contours of a highly deformed rotating compact star

In Fig. 2, contours of metric potentials and matter distribution in meridional (xz) and equatorial (xy) planes are presented. Also presented is the 3D density map of the stellar surface. The solution in Fig. 2 corresponds to a stationary axisymmetric differentially rotating compact star, whose parameter is DR1 in Table IV. The solution is highly deformed as the ratio of polar to equatorial radius in coordinate length to be $R_z/R_x=48/128=0.375$. Contours of p/ρ in the xz plane (left panel) show that the density distribution is toroidal in the central region of the star, as is commonly found in the differentially rotating stars.

In Fig. 3, the same quantities are presented as in Fig. 2, but for the triaxially deformed uniformly rotating model. We will see in a later section that the nonaxisymmetric deformation in coordinate becomes smaller as the compactness M/R is increased. We display a model with $M/R=0.2$, so that nonaxisymmetric deformation in the xy plane is evident. For this model, $R_y/R_x=100/128=0.78125$, and this is close to the maximally rotating configuration (the mass shedding limit), where the cusp is formed at the surface on the x axis.

Physical quantities for these selected models are tabulated in Table V. Definitions of listed integral quantities are summarized in the Appendix. It is noticeable that the virial integral to measure the accuracy of the solution $I_{\rm vir}/|\mathcal{W}|$ is relatively large, ~ 0.07 for the DR1 model. This is one of the least accurate models in our whole set of computations. For most of the solutions, we find $I_{\rm vir}/|\mathcal{W}|\lesssim 10^{-4}$, and $I_{\rm vir}/|\mathcal{W}|\sim 10^{-3}$ for relatively inaccurate cases. $I_{\rm vir}/|\mathcal{W}|$ becomes $\sim 10^{-2}$ for extremely compact models $M/R\sim 0.3$ under a stiff EOS $\Gamma\gtrsim 3$ and a large deformation due to the differential rotation.

[6]Such an excess of the maximum mass occurs even when the rotating star maintains a spherical topology. When the star has enough angular momentum to become a toroidal shape, the maximum mass becomes much higher [30].

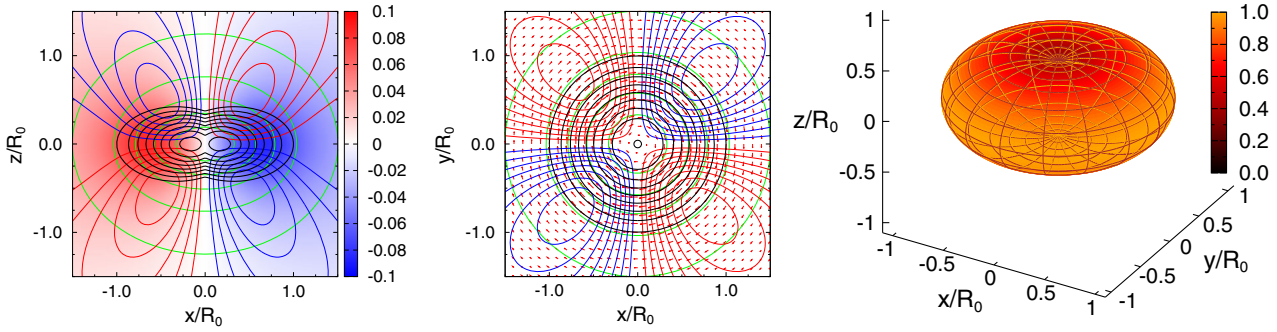

FIG. 2. An axisymmetric equilibrium of a differentially rotating compact star. Parameters of the presented model are $\Gamma = 3$, $M/R = 0.3$, $q = 4$, $A/R_0 = 10^{-3/2}$, and $R_z/R_x = 48/128$ (see DR1 in Table IV). Left panel: Quantities in the meridional (xz) plane. Contours are for p/ρ in every 0.02 (black), ψ in every 0.05 (green), and h_{xz} in every 0.005. Color density map indicates the y component of conformally weighted shift $\tilde{\beta}_y$. Center panel: Quantities in the equatorial (xy) plane. Contours are the same as the left panel, but the red and blue contours are for h_{xy} in every 0.005. Arrows denote the conformally weighted shift $\tilde{\beta}_i$. In the left and center panels, the value at the innermost contour of ψ corresponds to $\psi = 1.3$. Right panel: Surface of the compact star in coordinate radius. Color density map indicates $R(\theta,\phi)/R_0$, the coordinate radius $R(\theta,\phi)$ normalized by the equatorial radius (along the x axis) R_0.

3. Convergence tests

In Fig. 4, results of convergence tests are presented for the same differentially rotating and triaxially deformed models (DR1 and UR1 models in Table IV, respectively) as in the previous Sec. IV A 2. Grid setups for the convergence tests are listed in Table II. The resolution of grid spacing is increasingly higher from H1 to H4; at each level the resolution becomes double that of the previous level. Because of a limit of computational resources, we calculate the differentially rotating (DR1) model with the IWM formulation for H1–H4 resolutions, while we calculate the triaxially deformed (UR1) model with the same waveless formulation, but only for H1–H3 resolutions.

In the top panel of Fig. 4, the convergence of the virial integral $I_{\rm vir}/|\mathcal{W}|$ and the equality of $M_{\rm ADM}$ and $M_{\rm K}$ are presented. Here the ADM and Komar mass are computed both the volume integral formula in (A5) and (A7), and the surface integral formula in (A4) and (A8) for each mass. The resolution Δ here is represented by $1/N_r^{\rm f}$. As has been mentioned in the previous section as well as in the series of papers, second-order finite difference formulas (and partly third- or fourth-order formulas) are used in the COCAL code. In contrast to computations of black hole initial data [6], the surface of compact stars comes in between grid points when the field equations are integrated. This is likely to be a reason for the order of convergence becoming less than the second order (Δ^2 in the figures), especially when the adiabatic index of the EOS $\Gamma > 2$. We do not display other quantities, but overall, the numerical errors converge between the first and the second order in grid spacing Δ as shown in the top panel of Fig. 4. The error of the same quantities converges with higher order for model UR1 in the bottom panel. This may be because the solution is close to the mass shedding limit, and hence the increase of the resolution suddenly improves the accuracy of this particular solution.

TABLE IV. Model parameters of rotating compact stars. UR1–3 are for uniformly rotating models, and DR1–7 are for differentially rotating models. In this article, M/R of a rotating compact star is the compactness of a corresponding spherical solution having the same rest mass M_0. In the figure citations, "t", "m", and "b" after the numbers correspond to top, middle, and bottom panels, respectively.

Model	Figure	Γ	M/R	q	A/R_0	R_i/R_x ($i = z$ or y)
DR1	2, 4t	3	0.3	4	$10^{-3/2}$	48/128
DR2	5t	2	0.02 <	1	1	16/128–112/128
DR3	5b	3	0.14 <	1	1	16/128
DR4	5b	3	0.14 <	2	$10^{-3/2}$	16/128
DR5	5m, 5b	3	0.14 <	4	$10^{-3/2}$	40/128–112/128
DR6	5b	3	0.14 <	8	$10^{-3/2}$	56/128
DR7	5b	3	0.14 <	16	$10^{-3/2}$	64/128
UR1	3, 4b	4	0.2	···	···	100/128
UR2	5b	3	0.14 <	···	···	76/128
UR3	6	4	0.1–0.3	···	···	120/128–54/128

4. Comparisons of axisymmetric solutions

As a final check of the code, we briefly compare stationary and axisymmetric solutions of uniformly rotating compact stars computed by the present COCAL code with those computed by the other two well-known public domain codes, the LORENE library [32] and the RNS code [33]. In the COCAL code, we use the waveless formulation and compute a solution with H3 resolution. In the Nrotstar code of the LORENE library, three computational domains, among which one covers a star, are used, where the collocation points of each domain are set to (33,17) in (r,θ) coordinates. In the RNS code, we set the number of grid points as (401,201) in (r,θ) coordinates, and include multipoles up to $L = 12$.

In Table VI, comparisons of two models for the case with polytropic EOS $\Gamma = 3$ are shown. Gauge-invariant quantities except for the virial error are listed in the table. In

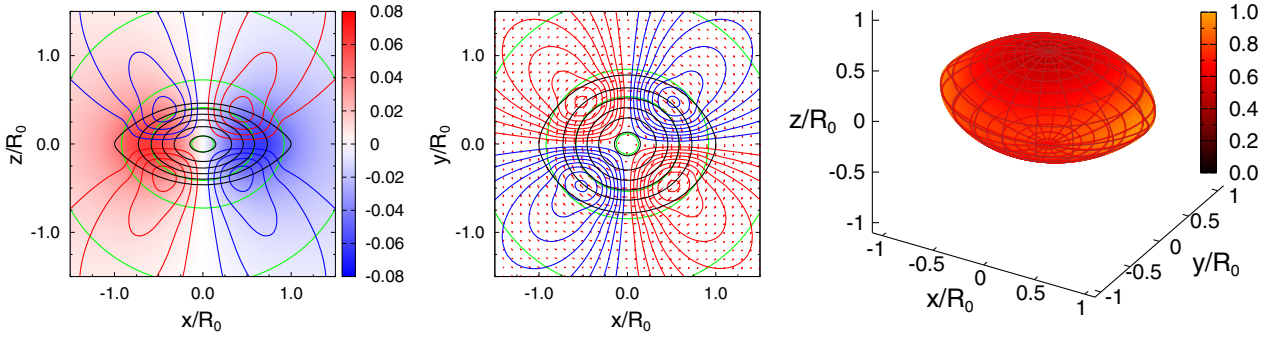

FIG. 3. The same as Fig. 2, but for triaxially deformed quasiequilibrium initial data of a rotating compact star. Parameters of the presented model are $\Gamma = 4$, and $M/R = 0.2$, $R_y/R_x = 100/128$ (UR1 in Table IV). Contours are drawn in the same manner as Fig. 2, except h_{xz} and h_{xy} are in every 0.0005 (red and blue) in the left and center panels, respectively. In the left and center panels, the value at the innermost contour of ψ corresponds to $\psi = 1.2$.

these solutions from three different codes, we set the central rest mass density ρ_c and the angular velocity Ω to be the same. The lower- and higher-ρ_c models shown in the left and right blocks of the table correspond to the $M/R = 0.2$ and 0.3 models, respectively. The rotation of presented models, $T/|W| \sim 0.1$, is not as rapid as the Kepler rotation near the equator, but it is rapid enough to largely deform the compact stars as much as the axis ratio $R_z/R_x \sim 0.7$.

In the LORENE and RNS codes, the metric for stationary axisymmetric and circular spacetime is solved. Because the waveless formulation should reproduce the stationary and axisymmetric spacetime, the gauge-independent quantities of solutions from these codes should agree. As shown in Table VI, the results of these two models agree fairly well. The largest difference is found to be about 1% in $T/|W|$ for the highly compact case with $M/R = 0.3$.

B. Differentially rotating stars with various rotation laws

We have computed sequences of differentially rotating axisymmetric solutions for selected parameters of the adiabatic index and differential rotation parameters $(\Gamma, q, A/R_0)$. Each curve plotted in Fig. 5 is a sequence of about 40 to 80 solutions. To reduce the computing time, we use IWM formulation in these calculations. Model parameters are listed in Table IV, and a resolution of computations are chosen to be H3.

In the top panel of Fig. 5, the rest mass M_0 is plotted against the maximum density ρ_c for the case with $\Gamma = 2$, $q = 1, A/R_0 = 1$. This parameter set is one of those used in BSS [28], which yielded the largest mass in their calculations. The solid curves in the panel from top to bottom correspond to solutions with the fixed axis ratio $R_z/R_0 = 0.125$ to 0.875 with steps of 0.125, and the dashed curve corresponds to the sequence of spherical solutions of Tolman-Oppenheimer-Volkov (TOV) equations for the case with $\Gamma = 2$. As seen in the panel, the amount of supported rest mass M_0 at a certain ρ_c increases as the axis ratio decreases (and accordingly the rotational kinetic energy or the total angular momentum increases). The maximum mass of the highly deformed differentially rotating object can be more than twice of that of the spherical TOV solution of the same EOS (see Table III), which agrees with the result reported in BSS [28].

The middle panel of Fig. 5 is the same as the top panel, but for the case with $\Gamma = 3$, $q = 4$, and $A/R_0 = 10^{-3/2}$. For the case with $q \gtrsim 4$, solution sequences of spheroidal stars with a given maximum density ρ_c and with decreasing R_z/R_0 are likely to terminate at a certain R_z/R_0, where the mass shedding from the equator occurs. We also notice that

TABLE V. Selected solutions of the stationary axisymmetric differentially rotating compact star, and the triaxially deformed uniformly rotating compact star. Definitions of listed quantities are as follows: $\bar{R}_x$, $\bar{R}_y$, and $\bar{R}_z$ are semimajor axes (radii along x, y, and z axes, respectively) measured in proper length, and $\bar{R}_0 = \bar{R}_x$. ρ_c and p_c are the maximum values of the rest mass density and the pressure, respectively. The angular velocity Ω is the value at the rotation axis for the case with differential rotation, and is constant with the uniform rotation. It is normalized by the gravitational mass M of the spherical TOV solution of the same rest mass M_0. For the model DR1, $M = 1.829387$, and for UR1, $M = 1.313533$. The ADM mass $M_{\rm ADM}$, the rest mass M_0, the proper mass $M_{\rm P}$, the total angular momentum J, the ratio of the kinetic to gravitational energy $T/|W|$, and the normalized virial integral $I_{\rm vir}/|\mathcal{W}|$ are defined in the Appendix. All dimensional quantities are in $G = c = M_\odot = 1$ units. To convert the length unit to km, multiply $GM_\odot/c^2 = 1.47690$ km. In the computation, the parameter set H3 listed in Table II is used.

Model	$\bar{R}_0$	$\bar{R}_y/\bar{R}_x$	$\bar{R}_z/\bar{R}_0$	ρ_c	$(p/\rho)_c$	ΩM	$M_{\rm ADM}$	M_0	$M_{\rm P}$	J/M^2	$T/\lvert W\rvert$	$I_{\rm vir}/\lvert\mathcal{W}\rvert$
DR1 (Fig. 2)	10.276	0.99930	0.49673	0.0017764	0.15091	0.50677	1.97872	2.21005	2.28802	0.94867	0.1974	7.27×10^{-2}
UR1 (Fig. 3)	10.969	0.79585	0.48802	0.0013849	0.10576	0.053378	1.35569	1.50000	1.52105	0.93972	0.1661	6.96×10^{-6}

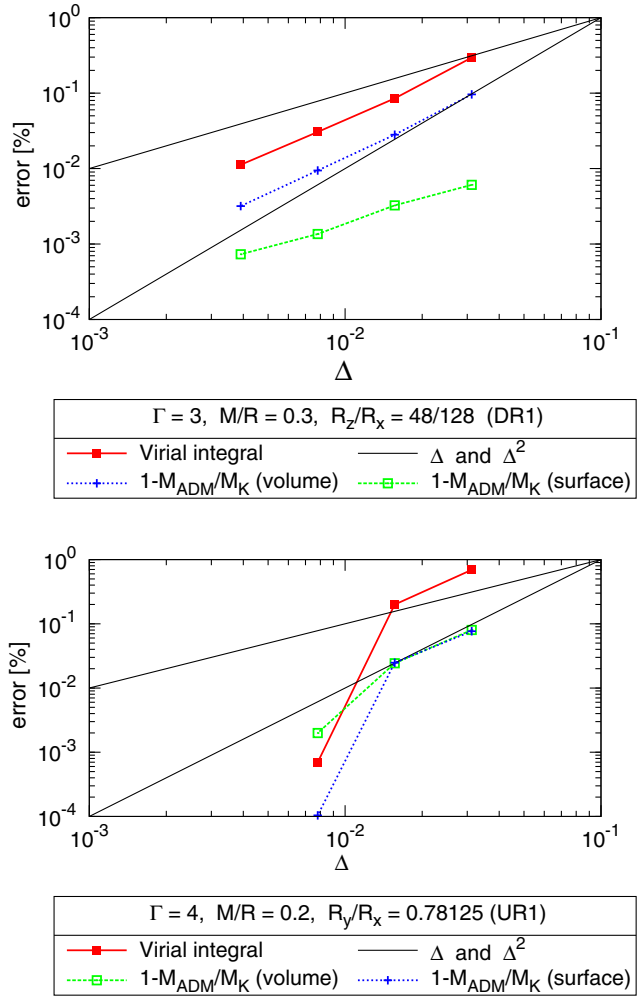

FIG. 4. Result of convergence tests for the virial integral and the equality of $M_{\rm ADM}$ and $M_{\rm K}$. Top panel: Differentially rotating model calculated with resolutions H1–H4. Model parameters are the same as the model in Fig. 2, but the IWM formulation is used in these computations. Bottom panel: Uniformly rotating triaxial model calculated with resolutions H1–H3. Model parameters are the same as the model in Fig. 3, and the waveless formulation is used in these computations.

the sequences with a fixed smaller R_z/R_0 do not extend to higher maximum density, also because of the mass shedding.

For the compressible matter with Γ in the range of our interest in this article $\Gamma \sim 2-4$, uniformly rotating sequences parametrized by the axis ratio R_z/R_0 terminate at the mass shedding limit at a certain value around $R_z/R_0 \sim 0.5-0.65$.[7] The maximum mass of a rotating solution with such a breakup velocity is known to exceed $\lesssim$20% of the maximum mass of the spherical TOV solution [3]. Differential rotation can support larger masses than the uniform rotation because of two properties. One is that the differential rotation tends to redistribute the density near the central region in the toroidal shape (see the left panel of Fig. 2), hence it reduces the density of the core. The other is that the drop in angular velocity decreases the centrifugal force near the equatorial surface, which prevent the mass shedding.

In the bottom panel of Fig. 5, curves of $M_0(\rho_c)$ are plotted for a set of various differential rotation parameters $(q, A/R_0)$ for the case with $\Gamma = 3$ EOS. Each curve corresponds to the smallest R_z/R_0 of the present computation for each parameter set. We calculate models for $q = 2$, 4, 8, and 16 with a small transition parameter $(A/R_0)^2 = 0.001$ to see the effect of the slope of a rotation profile (see Sec. IV A 1). The curves for $q = 4$, 8, and 16 are close to the maximally rotating models (mass shedding limit), whose axis ratios R_z/R_0 are $0.3125(= 40/128)$, $0.4375(= 56/128)$, and $0.5(= 64/128)$, respectively. As mentioned above, in this range of q, spheroidal sequences terminate at the mass shedding limit with increasing deformation. Excesses of the rest mass M_0 compared to that of the spherical TOV solution (that of the uniformly rotating solution with $R_z/R_0 = 0.59375$) are 46.8% (23.0%), 31.6% (10.3%), and 25.1% (4.81%) for $q = 4$, 8, and 16, respectively.

In contrast, for the model with $q = 2$, the equilibrium solution sequence continues from a spheroidal to a toroidal one without being subject to the mass shedding. As seen in the bottom panel of Fig. 5, the curve with $q = 2$, however, has a smaller axis ratio $R_z/R_0 = 0.125(= 16/128)$; the excess of the maximum rest mass is smaller than that of the other cases, $q = 4$, 8, and 16, as well as that of uniform rotation. Apparently, for $q \lesssim 2$ a much higher excess of the maximum mass would appear when the configuration becomes toroidal. Hence, we expect that the equilibriums of differentially rotating compact stars dramatically change as the slope parameter varies from $q = 2$ and 4.

In the bottom panel of Fig. 5, we also plot a model with a larger transition parameter $A/R_0 = 1$ for a comparison. This model has the same set of rotation parameters $(q, A/R_0, R_z/R_0) = (1, 1, 0.125)$ as the top curve of the top panel, but it is computed for the stiffer EOS $\Gamma = 3$. This rotation parameter provides a large excess of the maximum rest mass also, consistent with the result in BSS [28]. We mention that this rotation law with $q = 1$ corresponds to the so-called j-constant law, but with such a large $A/R_0 = 1$, the specific angular momentum is not distributed constantly in the region $r \lesssim R_0$, even in the Newtonian limit.

C. Triaxially deformed solutions in waveless formulation

In Fig. 6, we present results of uniformly rotating solutions. Sequences of stationary axisymmetric equilibriums as well as triaxially deformed quasiequilibrium initial data are computed from the code for the waveless formulation and compared with those from the IWM formulation [5]. Since a sequence of triaxial solutions is

[7]This value may be larger for softer EOS with $\Gamma < 2$ (smaller for stiffer EOS with $\Gamma > 4$).

TABLE VI. Comparisons of the uniformly rotating compact stars computed by three different numerical codes. The polytropic EOS with $\Gamma = 3$ listed in Table III is used. The left and right blocks of data are for $M/R = 0.2$ and 0.3, respectively. The angular velocity is large enough to deform the compact star as much as the axis ratio $R_z/R_x \sim 0.7$. Values of $I_{\rm vir}/|\mathcal{W}|$ of LORENE are those of GRV3 (see e.g. Ref. [4]). $G = c = M_\odot = 1$ units are used except for the rotational frequency $\Omega/2\pi$.

Model	$\rho_c = 0.00167505$ $\Omega/2\pi = 1186.12$ Hz					$\rho_c = 0.00250814$ $\Omega/2\pi = 1512.18$ Hz				
Code	M_0	$M_{\rm ADM}$	J	$T/\lvert W\rvert$	$I_{\rm vir}/\lvert\mathcal{W}\rvert$	M_0	$M_{\rm ADM}$	J	$T/\lvert W\rvert$	$I_{\rm vir}/\lvert\mathcal{W}\rvert$
LORENE	1.50006	1.34846	1.18851	0.101117	3.11803×10^{-6}	2.20607	1.88755	2.17978	0.102008	-1.91164×10^{-6}
RNS	1.49978	1.34820	1.18793	0.101106	⋯	2.20597	1.88739	2.17909	0.101991	⋯
COCAL	1.50000	1.34855	1.18804	0.101381	3.39518×10^{-6}	2.21005	1.89167	2.18532	0.103053	7.95317×10^{-4}

known to extend longer (as the deformation becomes larger) for a larger adiabatic index Γ, it is chosen to be $\Gamma = 4$ in this calculation.

In Fig. 6, plotted are the ratio of kinetic energy to the gravitational energy, $T/|W|$, against the eccentricity $e \coloneqq \sqrt{1-(\bar{R}_z/\bar{R}_x)^2}$ in proper length for constant rest-mass sequences with three different compactness parameters $M/R = 0.1$, 0.2, and 0.3. Curves extending from $e \sim 0.3$ in top panels correspond to axisymmetric sequences (labeled with ML), and short horizontal branches correspond to triaxially deformed sequences (labeled with JB). The short branches in the inset of the top panel are shown in a zoomed-in view in the bottom panel of Fig. 6, and are plotted together with the result from IWM formulation. The $T/|W|$ of each triaxially deformed sequence is nearly constant; its difference between the waveless and IWM formalism is negligible for the mildly compact case $M/R = 0.1$ and increases as M/R.

Bonazzola, Frieben, and Gourgoulhon [34] have developed a method to locate a point along a solution sequence where a secular instability sets in. The method has been applied to locate Jacobi-like bar mode instability points on solution sequences of relativistic homogeneous fluids [35], strange stars [36], and relativistic polytropes [37]. For the relativistic homogeneous fluid, a dependence of $(T/|W|)_{\rm crit}$, the value of $T/|W|$ at the secular instability point, on the compactness M/R is found to be approximated by the function

$$(T/|W|)_{\rm crit} \simeq (T/|W|)_{\rm crit,Newt} + 0.126(M/R)(1+M/R), \qquad (70)$$

where $(T/|W|)_{\rm crit,Newt} \simeq 0.1375$ is the value of Newtonian limit [35]. Notwithstanding a difference in the EOS, values of $T/|W|$ at the bifurcation points in the bottom panel of Fig. 6 agree fairly well with the values from the function (70), except for the case with $M/R = 0.3$. Another result from Ref. [37] that could be compared with our results is the value of $(T/|W|)_{\rm crit} = 0.1507$ for the case with $\Gamma = 2.9$ and $M/R = 0.1$.

V. DISCUSSION

The value of $T/|W|$ has been used as a criterion for a certain instability to set in. It has often been observed that the fastest growing secular instability of polar parity oscillation ($\ell = m = 2$ f-mode) due to the gravitational radiation [Chandrasekhar-Friedman-Schutz (CFS) instability [38]] or viscosity [39,40] sets in around $T/|W| \sim 0.14$, and that the rotating star becomes dynamically unstable around $T/|W| \sim 0.27$. These numbers were treated as magic numbers, as they weakly depend on the stiffness of EOSs (such as the polytropic index) for uniformly rotating stars in Newtonian gravity.

However, recent simulations and eigenmode analysis of rotating compact stars for a wide range of compactness M/R, EOSs, and differential rotation parameters, clarified that the critical value $(T/|W|)_{\rm crit}$ depends on these parameters. For uniformly rotating compact stars, zero-frequency $\ell = m$ f-mode perturbation appears at lower (higher) values $(T/|W|)_{\rm crit}$ for retrograde (prograde) modes as the compactness M/R increases [41–44]. This includes the increase of $(T/|W|)_{\rm crit}$ at the $\ell = m = 2$ bifurcating point of triaxially deformed solutions (Jacobi sequences) with the increase of M/R as seen in Fig. 6 (see also Refs. [34,45]). Such solutions, however, are interesting only if the viscosity of high-density matter is fairly strong, so that its time scale is much shorter than that of damping time due to gravitational wave emission.

Differential rotation also affects the critical value $(T/|W|)_{\rm crit}$. That of the above mentioned CFS instability of bar mode may be as small as 0.1 for differentially rotating stars in Newtonian gravity [46]. Also in Newtonian gravity, critical $T/|W|$ of the dynamical bar mode instability is reported to be as low as 0.23 for a relatively moderate differential rotation ($q = 1$, $A/R_0 = 0.7$), compared to 0.27 for a uniformly rotating star [47] (see also Ref. [48]). When the rotation profile is strongly differential as $A/R_0 \sim 0.1 - 0.3$, potentially new nonaxisymmetric dynamical instability sets in at values as small as $(T/|W|)_{\rm crit} \sim 0.01$ [49]. It is of great importance to investigate the effect of relativistic gravity on these critical configurations with differential rotation. Solutions computed from our new COCAL code can be applied to mode analysis of the differentially rotating compact stars such as that in Ref. [44].

On the other hand, the axisymmetric dynamical instability of rotating compact stars has not yet been fully investigated. The issue is related to the onset of collapse of

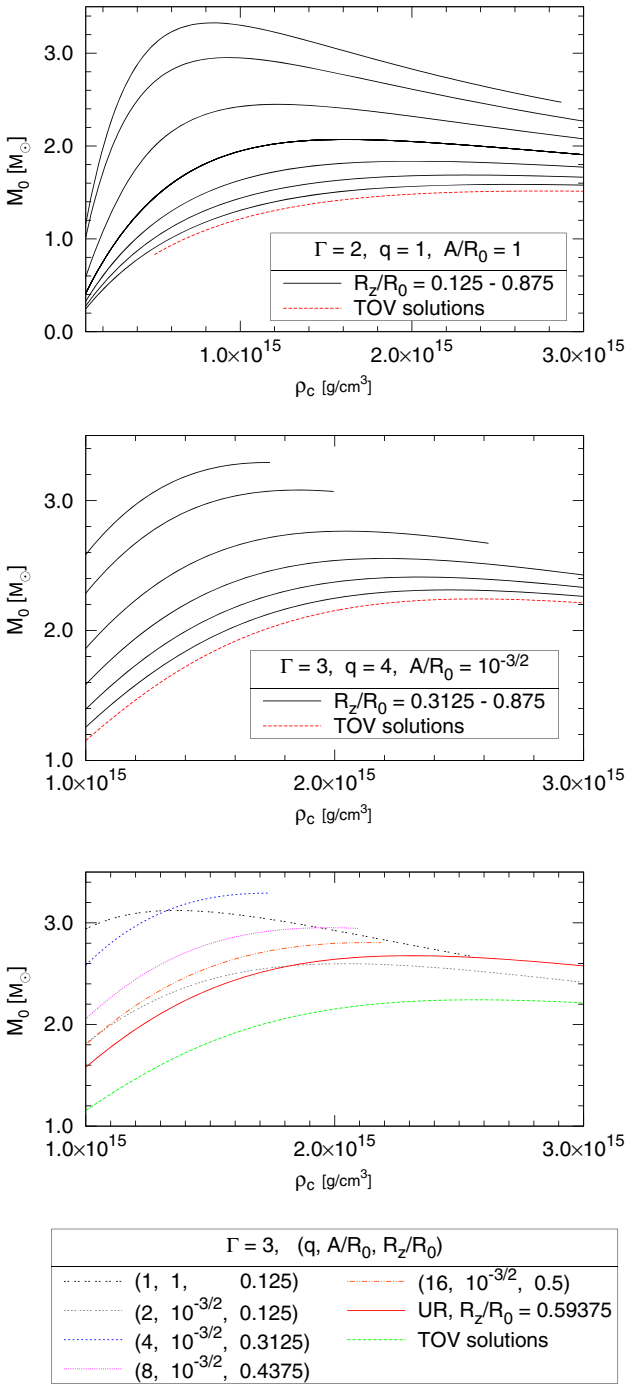

FIG. 5. Sequences of axisymmetric differentially rotating compact stars in equilibrium. The rest mass–maximum density $M_0(\rho_c)$ curves are plotted for a certain axis ratio R_z/R_0. Top panel: The case with $\Gamma = 2$, $q = 1$, $A/R_0 = 1$. The solid curves in the panel from top to bottom correspond to solutions with the axis ratios $R_z/R_0 = 0.125$ to 0.875 with steps of 0.125. Middle panel: The case with $\Gamma = 3$, $q = 4$, $A/R_0 = 10^{-3/2}$. The solid curves in the panel from top to bottom correspond to solutions with the axis ratio $R_z/R_0 = 0.3125$, and 0.375 to 0.875 with steps of 0.125. Bottom panel: Sequences for various rotation parameters $(q, A/R_0, R_z/R_0)$. Each curve corresponds to the largest deformation (the smallest R_z/R_0) of the present computation. A solid curve labeled with UR is a result for the uniformly rotating sequence.

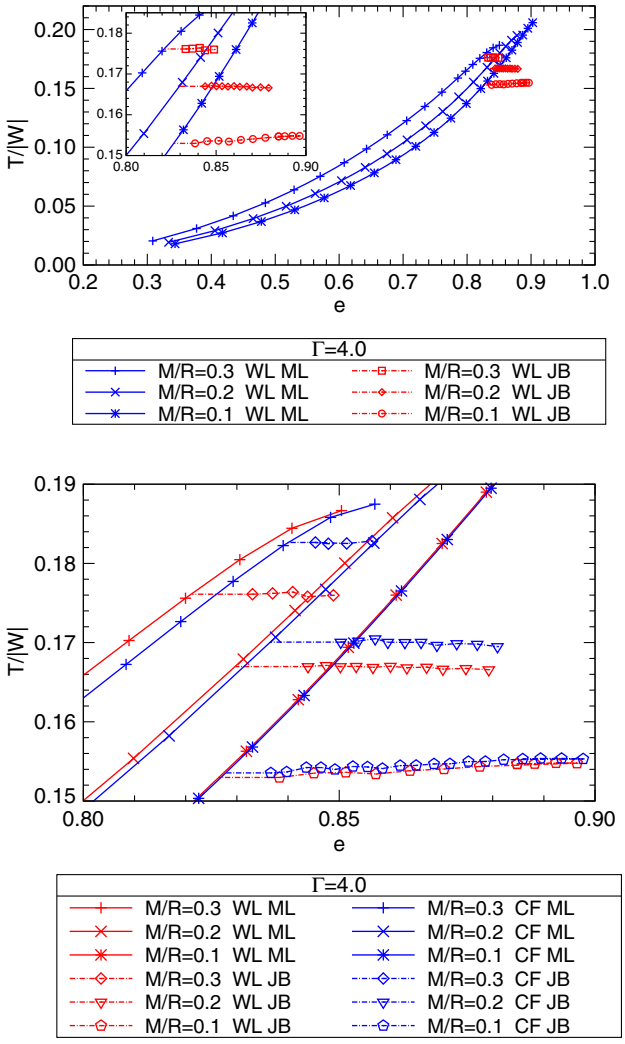

FIG. 6. Constant rest mass sequences for uniformly rotating compact stars. The ratio of the kinetic to the gravitational energy $T/|W|$ is plotted against the eccentricity $e \coloneqq \sqrt{1-(\bar{R}_z/\bar{R}_x)^2}$ measured in the proper length. The adiabatic index is set at $\Gamma = 4$, and the resolution H2 is used. Top panel: Sequences computed with the waveless formulation. The curves labeled with ML are sequences of axially symmetric solutions, and those labeled JB are triaxially deformed solutions. Bottom panel: Same as top panel, but a closeup of the region near the branching points. The curves labeled with WL are sequences computed with the waveless formulation, and CF with the IWM formulation.

accreting neutron stars in evolved low-mass x-ray binaries or prompt collapse of a newly born neutron star in a core-collapse-type supernova. Takami *et al.* [50] showed by fully relativistic simulations that the onset of the axisymmetric dynamical instability of a uniformly rotating compact star is slightly before the secular instability point determined by the turning point method [51]. It is certainly interesting to investigate how the differential rotation changes the critical point of axisymmetric instability. Our new COCAL code again will be useful for preparing

equilibrium stellar models for perturbative studies as well as for initial data of such simulations.

For realistic high-density neutron star matter, it is more likely that the viscosity is negligibly weak so that instability due to the gravitational wave grows much faster than that of viscosity. If this is the case, the astrophysically relevant nonaxisymmetric solution is a Dedekind-type solution whose triaxial ($\ell = m = 2$) deformation is static, and is supported by its stationary internal flows (see results from simulations such as Ref. [52]). Also, with deformations corresponding to higher modes $\ell = m = 3$ or 4, branches of stationary solutions may bifurcate from axisymmetric sequences.

In the last 15 years, numerical relativity has been developed rapidly, and more sophisticated dynamical simulations have become possible, including those coupled with neutrino radiation or magnetic field evolutions. However, stationary or quasiequilibrium solutions of the outcome of such dynamical processes are still poorly modeled. A significance of the COCAL code is to provide high extensibility by adding more processes including magnetic fields, gravitational waves, and neutrino radiation in computations of stationary state. It is also available for computing nonaxisymmetric configurations, so that more interesting Dedekind-type or other systems as an outcome of CFS instability can be calculated in the future. Our development of the single-star code presented in this paper is to prepare a basis of such code for increasingly complex modeling of realistic compact stars in the future.

Also in the COCAL code, a solution is calculated on a spatial hypersurface Σ_t under gauge conditions similar to those used in standard numerical relativity simulations of compact objects. Hence, it is more straightforward to prepare initial data for the simulations as well as to model the outcome of the simulations. Recent implementation [53] of a COCAL driver in simulation code like the ones based on the CACTUS [54] infrastructure will streamline such modeling of differentially rotating hypermassive neutron stars.

ACKNOWLEDGMENTS

This work was supported by a JSPS Grant-in-Aid for Scientific Research (C), Grants No. 23540314, No. 15K05085, No. 26400267, and No. 25400262. F. G. is supported by the Helmholtz International Center for FAIR within the framework of the LOEWE program launched by the State of Hesse. A. T. thanks to Vibetech Consultants LLC for a support.

APPENDIX: DEFINITIONS FOR INTEGRAL QUANTITIES

In this appendix, we summarize definitions of physical quantities for rotating compact stars (see e.g. Refs. [4,55]), which are tabulated for selected solutions in Table V. An archive of numerical data used in the top and middle panels of Fig. 5, and in Fig. 6, is provided as associated Supplemental Material of this article [56].

In Table V, $\bar{R}_0 (= \bar{R}_x)$, $\bar{R}_y$, and $\bar{R}_z$ are the radii of a compact star along the x, y, and z axes, in the proper length,

$$\bar{R}_i := \int_0^{R_i} \psi^2 \sqrt{\tilde{\gamma}_{ii}} dx^i. \tag{A1}$$

Here summation is not taken over the index $i (= x, y, z)$, and the unbarred R_i represents the coordinate radii along each axis.

The rest mass M_0 and the proper mass $M_{\rm P}$ are defined, respectively, as follows:

$$M_0 := \int_\Sigma \rho u^\alpha dS_\alpha = \int_\Sigma \rho u^t \alpha \psi^6 \sqrt{\tilde{\gamma}} d^3x, \tag{A2}$$

$$M_{\rm P} := \int_\Sigma \epsilon u^\alpha dS_\alpha = \int_\Sigma \epsilon u^t \alpha \psi^6 \sqrt{\tilde{\gamma}} d^3x, \tag{A3}$$

where $dS_\alpha = \nabla_\alpha t \sqrt{-g} d^3x$, and $d^3x = r^2 \sin\theta dr d\theta d\phi$ on the spherical coordinates. Apparently a volume integral over the hypersurface Σ is nonzero only on the fluid support.

The ADM mass $M_{\rm ADM}$ is defined and calculated by

$$M_{\rm ADM} := \frac{1}{16\pi} \int_\infty (f^{ac} f^{bd} - f^{ab} f^{cd}) \mathring{D}_b \gamma_{cd} dS_a$$
$$= -\frac{1}{2\pi} \int_\infty \tilde{D}^a \psi d\tilde{S}_a \tag{A4}$$
$$= \frac{1}{2\pi} \int_\Sigma \left[-\frac{\psi}{8} {}^3\tilde{R} + \frac{1}{8} \psi^5 \left(\tilde{A}_{ab} \tilde{A}^{ab} - \frac{2}{3} K^2 \right) + 2\pi \psi^5 \rho_{\rm H} \right] \sqrt{\tilde{\gamma}} d^3x, \tag{A5}$$

where both the surface integral (A4) and the volume integral (A5) are evaluated for the ADM mass to cross-check the accuracy of numerics. We calculate approximate values of this surface integral on a sphere with a large radius, about $r \sim 10^4 R_0$. Note that at spatial infinity $\tilde{\gamma}^{ab} \to f^{ab}$, $\tilde{D}_a \to D_a$, and $d\tilde{S}_a = \nabla_a r \sqrt{\tilde{\gamma}} d^2x = \nabla_a r \sqrt{f} d^2x = dS_a$; we may replace the surface integral with that of flat coordinates within a negligible numerical error.

The Komar mass associated with a globally defined timelike Killing field t^α,

$$M_{\rm K} := -\frac{1}{4\pi} \int_\infty \nabla^\alpha t^\beta dS_{\alpha\beta} \tag{A6}$$
$$= \int_\Sigma (2T^\alpha{}_\beta - T g^\alpha{}_\beta) t^\beta dS_\alpha$$
$$= \int_\Sigma [\alpha(\rho_{\rm H} + S) - 2 j_a \beta^a] \psi^6 \sqrt{\tilde{\gamma}} d^3x, \tag{A7}$$

and the asymptotic Komar mass whose t^α is a symmetry of an asymptotically flat spacetime,

$$M_{\rm K} := -\frac{1}{4\pi}\int_\infty \nabla^\alpha t^\beta dS_{\alpha\beta} = \frac{1}{4\pi}\int_\infty D^a\alpha dS_a \quad \text{(A8)}$$

$$= \frac{1}{4\pi}\int_\Sigma \left[\tilde{A}_{ab}\tilde{A}^{ab} + \frac{1}{3}K^2 - \pounds_n K + 4\pi(\rho_{\rm H} + S)\right]\alpha\psi^6\sqrt{\tilde{\gamma}}d^3x, \quad \text{(A9)}$$

should give the same value irrespective of the system being stationary and axisymmetric or not, when the waveless condition (13), the maximal slicing gauge $K = 0$, and the asymptotic falloff of metric potentials [Eqs. (14) and (15)] are imposed (see also Ref. [18]). We compute Eqs. (A7), (A8), and (A9) to check the consistency of the solutions. In the above, $(G_{\alpha\beta} - 8\pi T_{\alpha\beta})(\gamma^{\alpha\beta} + n^\alpha n^\beta) = 0$ is used to derive (A9).

Also for the angular momentum, the surface and the volume integrals are evaluated:

$$J := \frac{1}{8\pi}\int_\infty K^a{}_b\phi^b dS_a \quad \text{(A10)}$$

$$= \frac{1}{8\pi}\int_\Sigma D_a(K^a{}_b\phi^b)dV = \frac{1}{8\pi}\int_\Sigma \left(8\pi j_a\phi^a + A^a{}_b\tilde{D}_a\phi^b + \frac{2}{\psi}K\phi^a\overset{\circ}{D}_a\psi\right)\times\psi^6\sqrt{\tilde{\gamma}}d^3x. \quad \text{(A11)}$$

The values of $M_{\rm ADM}$ and J listed in Table V are those of volume integrals, (A5) and (A11). In Fig. 4, plotted masses are calculated from Eqs. (A5) and (A7) for volume integrals, and Eqs. (A4) and (A8) for surface integrals of $M_{\rm ADM}$ and $M_{\rm K}$, respectively.

For computing the ratio of the kinetic energy and the gravitational energy, $T/|W|$, we define, as in previous works [4],

$$W := M_{\rm ADM} - M_{\rm P} - T, \quad \text{(A12)}$$

$$T := \frac{1}{2}\int_\Sigma \Omega dJ. \quad \text{(A13)}$$

For the computation of kinetic energy, when the vector ϕ^a is a Killing field, the volume integral over Σ is again only over the fluid supports, and hence $dJ := j_a\phi^a\psi^6\sqrt{\tilde{\gamma}}d^3x$. When we compute Jacobi-type solutions, whose spacetimes are not axisymmetric, we still use this definition but set $T = \frac{1}{2}\Omega J$ for $\Omega =$ constant.

The relativistic virial theorem for perfect fluid spacetimes [57] is used to measure the accuracy of solutions. It is a vanishing integral of a spatial trace of Einstein's equations,

$$\int_\Sigma \left(T_a{}^a - \frac{1}{8\pi}G_a{}^a\right)dV = 2\mathcal{T} + 3\Pi + \mathcal{W} + M_{\rm ADM} - M_{\rm K} = 0, \quad \text{(A14)}$$

over a hypersurface Σ. An equality of the ADM mass and the Komar mass $M_{\rm ADM} = M_{\rm K}$ has been established in Ref. [58] for stationary spacetimes, and in Ref. [18] for waveless formulation. In the Newtonian limit, the integrals $\mathcal{T}$, Π, and $\mathcal{W}$ become the kinetic, internal, and gravitational energies, defined by

$$\mathcal{T} = \frac{1}{2}\int_\Sigma (\epsilon + p)u_a u^a dV, \quad \text{(A15)}$$

$$\Pi = \int_\Sigma p dV, \quad \text{(A16)}$$

$$\mathcal{W} = \frac{1}{4\pi}\int_\Sigma [\psi^{-4}(2\tilde{D}^a\ln\psi\tilde{D}_a\ln\psi - \tilde{D}^a\ln\alpha\tilde{D}_a\ln\alpha) + \frac{3}{4}\left(A_{ab}A^{ab} - \frac{2}{3}K^2\right) + \frac{1}{\alpha}K\beta^a\tilde{D}_a\ln\alpha + \frac{1}{4}{}^3\tilde{R}\psi^{-4}]dV. \quad \text{(A17)}$$

We define virial integral $I_{\rm vir}$ as

$$I_{\rm vir} = |2\mathcal{T} + 3\Pi + \mathcal{W}|. \quad \text{(A18)}$$

Note that the above defined T and W differ from $\mathcal{T}$ and $\mathcal{W}$ in the strong gravity regime.

[1] S. Bonazzola and G. Maschio, in *Proceedings from IAU Symposium No. 46 Jodrell Bank, England, 1970* (International Astronomical Union, Dordrecht, Netherlands, 1971), p. 346; S. Bonazzola and J. Schneider, Astrophys. J. **191**, 273 (1974); J. R. Wilson, Astrophys. J. **176**, 195 (1972); J. M. Bardeen, Astrophys. J. **162**, 71 (1970); E. M. Butterworth and J. R. Ipser, Astrophys. J. **200**, L103 (1975); Astrophys. J. **204**, 200 (1976);

J. L. Friedman, L. Parker, and J. R. Ipser, Astrophys. J. **304**, 115 (1986); N. Stergioulas and J. L. Friedman, Astrophys. J. **444**, 306 (1995); S. Bonazzola, E. Gourgoulhon, and J. A. Marck, Phys. Rev. D **58**, 104020 (1998); T. Nozawa, N. Stergioulas, E. Gourgoulhon, and Y. Eriguchi, Astron. Astrophys. Suppl. Ser. **132**, 431 (1998); M. Ansorg, A. Kleinwachter, and R. Meinel, Astron. Astrophys. **381**, L49 (2002); **405**, 711 (2003); M. Ansorg, T. Fischer, A. Kleinwachter, R. Meinel, D. Petroff, and K. Schobel, Mon. Not. R. Astron. Soc. **355**, 682 (2004).

[2] I. Hachisu, Astrophys. J. Suppl. Ser. **62**, 461 (1986); **61**, 479 (1986); H. Komatsu, Y. Eriguchi, and I. Hachisu, Mon. Not. R. Astron. Soc. **237**, 355 (1989).

[3] G. B. Cook, S. L. Shapiro, and S. A. Teukolsky, Astrophys. J. **398**, 203 (1992); S. L. Shapiro, S. A. Teukolsky, and T. Nakamura, Astrophys. J. **357**, L17 (1990); G. B. Cook, S. L. Shapiro, and S. A. Teukolsky, Astrophys. J. **422**, 227 (1994); **423**, L117 (1994); **424**, 823 (1994); D. Gondek-Rosinska, T. Bulik, L. Zdunik, E. Gourgoulhon, S. Ray, J. Dey, and M. Dey, Astron. Astrophys. **363**, 1005 (2000).

[4] J. L. Friedman and N. Stergioulas, *Rotating Relativistic Stars* (Cambridge University Press, Cambridge, England, 2013); N. Straumann, *General Relativity* (Springer Science and Business Media, Dordrecht, Netherlands, 2013); N. Stergioulas, Living Rev. Relativity **6**, 3 (2003); R. Meinel, M. Ansorg, A. Kleinwächter, G. Neugebauer, and D. Petroff, *Relativistic Figures of Equilibrium* (Cambridge University Press, New York, 2008).

[5] X. Huang, C. Markakis, N. Sugiyama, and K. Uryu, Phys. Rev. D **78**, 124023 (2008).

[6] K. Uryu and A. Tsokaros, Phys. Rev. D **85**, 064014 (2012); K. Uryu, A. Tsokaros, and P. Grandclement, Phys. Rev. D **86**, 104001 (2012); A. Tsokaros and K. Uryū, J. Eng. Math. **82**, 133 (2013).

[7] K. Uryu, E. Gourgoulhon, C. M. Markakis, K. Fujisawa, A. Tsokaros, and Y. Eriguchi, Phys. Rev. D **90**, 101501 (2014).

[8] A. Tsokaros, K. Uryu, and L. Rezzolla, Phys. Rev. D **91**, 104030 (2015).

[9] K. Ioka and M. Sasaki, Phys. Rev. D **67**, 124026 (2003); Astrophys. J. **600**, 296 (2004).

[10] R. Birkl, N. Stergioulas, and E. Muller, Phys. Rev. D **84**, 023003 (2011).

[11] e. g., J. L. Houser and J. M. Centrella, Phys. Rev. D **54**, 7278 (1996); K. C. B. New, J. M. Centrella, and J. E. Tohline, Phys. Rev. D **62**, 064019 (2000); J. D. Brown, Phys. Rev. D **62**, 084024 (2000); M. Saijo, M. Shibata, T. W. Baumgarte, and S. L. Shapiro, Astrophys. J. **548**, 919 (2001); M. Shibata, S. Karino, and Y. Eriguchi, Mon. Not. R. Astron. Soc. **334**, L27 (2002); **343**, 619 (2003).

[12] M. Shibata and Y. i. Sekiguchi, Phys. Rev. D **71**, 024014 (2005).

[13] M. Shibata and K. Uryū, Phys. Rev. D **61**, 064001 (2000).

[14] e. g., M. Shibata and K. Uryū, Phys. Rev. D **61**, 064001 (2000); Prog. Theor. Phys. **107**, 265 (2002); M. Shibata, K. Taniguchi, and K. Uryū, Phys. Rev. D **68**, 084020 (2003); **71**, 084021 (2005); Y. T. Liu, S. L. Shapiro, Z. B. Etienne, and K. Taniguchi, Phys. Rev. D **78**, 024012 (2008).

[15] J. Isenberg, Int. J. Mod. Phys. D **17**, 265 (2008); J. Isenberg and J. Nester, in *General Relativity and Gravitation* Vol. 1, edited by A. Held (Plenum Press, New York, 1980); J. R. Wilson and G. J. Mathews, in *Frontiers in Numerical Relativity*, edited by C. R. Evans, L. S. Finn, and D. W. Hobill (Cambridge University Press, Cambridge, England, 1989), p. 306.

[16] G. B. Cook, Living Rev. Relativity **3**, 5 (2000).

[17] e. g. N. Moldenhauer, C. M. Markakis, N. K. Johnson-McDaniel, W. Tichy, and B. Brügmann, Phys. Rev. D **90**, 084043 (2014).

[18] M. Shibata, K. Uryu, and J. L. Friedman, Phys. Rev. D **70**, 044044 (2004); **70**, 129901(E) (2004).

[19] K. Uryu, F. Limousin, J. L. Friedman, E. Gourgoulhon, and M. Shibata, Phys. Rev. Lett. **97**, 171101 (2006); K. Uryu, F. Limousin, J. L. Friedman, E. Gourgoulhon, and M. Shibata, Phys. Rev. D **80**, 124004 (2009); S. Bonazzola, E. Gourgoulhon, P. Grandclement, and J. Novak, Phys. Rev. D **70**, 104007 (2004).

[20] G. B. Cook, S. L. Shapiro, and S. A. Teukolsky, Phys. Rev. D **53**, 5533 (1996).

[21] F. Galeazzi, S. Yoshida, and Y. Eriguchi, Astron. Astrophys. **541**, A156 (2012).

[22] P. Mach and E. Malec, Phys. Rev. D **91**, 124053 (2015).

[23] E. Müller and Y. Eriguchi, Astron. Astrophys. **152**, 325 (1985).

[24] J. S. Read, B. D. Lackey, B. J. Owen, and J. L. Friedman, Phys. Rev. D **79**, 124032 (2009); J. S. Read, C. Markakis, M. Shibata, K. Uryu, J. D. E. Creighton, and J. L. Friedman, Phys. Rev. D **79**, 124033 (2009); B. D. Lackey, K. Kyutoku, M. Shibata, P. R. Brady, and J. L. Friedman, Phys. Rev. D **89**, 043009 (2014).

[25] J. P. Ostriker and J. W.-K. Mark, Astrophys. J. **151**, 1075 (1968).

[26] R. H. Price, C. Markakis, and J. L. Friedman, J. Math. Phys. (N.Y.) **50**, 073505 (2009).

[27] K. Uryū and Y. Eriguchi, Phys. Rev. D **61**, 124023 (2000); K. Uryū, M. Shibata, and Y. Eriguchi, Phys. Rev. D **62**, 104015 (2000); K. Uryū, F. Limousin, J. L. Friedman, E. Gourgoulhon, and M. Shibata, Phys. Rev. Lett. **97**, 171101 (2006).

[28] T. W. Baumgarte, S. L. Shapiro, and M. Shibata, Astrophys. J. **528**, L29 (2000).

[29] I. A. Morrison, T. W. Baumgarte, and S. L. Shapiro, Astrophys. J. **610**, 941 (2004).

[30] M. Ansorg, D. Gondek-Rosinska, and L. Villain, Mon. Not. R. Astron. Soc. **396**, 2359 (2009); M. Szkudlarek, D. Gondek-Rosińska, M. Ansorg, and L. Villain, *XXXVI Polish Astronomical Society Meeting, Warsaw, 2013* (Polish Astronomical Society, Warsaw, 2014), p. 132.

[31] W. Kastaun and F. Galeazzi, Phys. Rev. D **91**, 064027 (2015).

[32] http://www.lorene.obspm.fr/.

[33] http://www.gravity.phys.uwm.edu/rns/.

[34] S. Bonazzola, J. Frieben, and E. Gourgoulhon, Astrophys. J. **460**, 379 (1996); Astron. Astrophys. **331**, 280 (1998).

[35] D. Gondek-Rosinska and E. Gourgoulhon, Phys. Rev. D **66**, 044021 (2002).

[36] D. Gondek-Rosinska, E. Gourgoulhon, and P. Haensel, Astron. Astrophys. **412**, 777 (2003).

[37] M. Saijo and E. Gourgoulhon, Phys. Rev. D **74**, 084006 (2006); Astrophys. Space Sci. **308**, 481 (2007).

[38] S. Chandrasekhar, Phys. Rev. Lett. **24**, 611 (1970); J. L. Friedman and B. F. Schutz, Astrophys. J. **222**, 281 (1978); Commun. Math. Phys. **62**, 247 (1978).
[39] P. H. Roberts and K. Stewartson, Astrophys. J. **137**, 777 (1963).
[40] R. A. James, Astrophys. J. **140**, 552 (1964).
[41] N. Stergioulas and J. L. Friedman, Astrophys. J. **492**, 301 (1998).
[42] C. Cutler and L. Lindblom, Astrophys. J. **385**, 630 (1992).
[43] S. Yoshida and Y. Eriguchi, Astrophys. J. **490**, 779 (1997).
[44] S. Yoshida, Phys. Rev. D **86**, 104055 (2012).
[45] S. L. Shapiro and S. Zane, Astrophys. J. **460**, 379 (1996).
[46] S. Karino and Y. Eriguchi, Astrophys. J. **578**, 413 (2002).
[47] S. Karino and Y. Eriguchi, Astrophys. J. **592**, 1119 (2003).
[48] M. Shibata, T. W. Baumgarte, and S. L. Shapiro, Astrophys. J. **542**, 453 (2000).
[49] M. Shibata, S. Karino, and Y. Eriguchi, Mon. Not. R. Astron. Soc. **343**, 619 (2003); **334**, L27 (2002).
[50] K. Takami, L. Rezzolla, and S. Yoshida, Mon. Not. R. Astron. Soc. **416**, L1 (2011).
[51] J. L. Friedman, J. R. Ipser, and R. D. Sorkin, Astrophys. J. **325**, 722 (1988).
[52] M. Shibata and S. Karino, Phys. Rev. D **70**, 084022 (2004).
[53] A. Tsokaros *et al.* (to be published).
[54] http://einsteintoolkit.org/.
[55] E. Gourgoulhon, *3+1 Formalism in General Relativity: Bases of Numerical Relativity* (Springer, Berlin, 2012).
[56] See Supplemental Material at http://link.aps.org/supplemental/10.1103/PhysRevD.93.044056 for an archive of physical quantities of numerical solutions presented in this article.
[57] E. Gourgoulhon and S. Bonazzola, Classical Quantum Gravity **11**, 443 (1994).
[58] R. Beig, Phys. Lett. A **69**, 153 (1978).